



Kent Academic Repository

Wozniakiewicz, Penelope J., Ishii, Hope A., Kearsley, Anton T., Bradley, John P., Price, Mark. C., Burchell, Mark J., Teslich, Nick and Cole, Mike J. (2015) *The survivability of phyllosilicates and carbonates impacting Stardust Al foils: Facilitating the search for cometary water*. *Meteoritics & Planetary Science*, 50 (12). pp. 2003-2023. ISSN 1086-9379.

Downloaded from

<https://kar.kent.ac.uk/56951/> The University of Kent's Academic Repository KAR

The version of record is available from

<https://doi.org/10.1111/maps.12568>

This document version

Publisher pdf

DOI for this version

Licence for this version

CC BY (Attribution)

Additional information

Versions of research works

Versions of Record

If this version is the version of record, it is the same as the published version available on the publisher's web site. Cite as the published version.

Author Accepted Manuscripts

If this document is identified as the Author Accepted Manuscript it is the version after peer review but before type setting, copy editing or publisher branding. Cite as Surname, Initial. (Year) 'Title of article'. To be published in **Title of Journal**, Volume and issue numbers [peer-reviewed accepted version]. Available at: DOI or URL (Accessed: date).

Enquiries

If you have questions about this document contact ResearchSupport@kent.ac.uk. Please include the URL of the record in KAR. If you believe that your, or a third party's rights have been compromised through this document please see our [Take Down policy](https://www.kent.ac.uk/guides/kar-the-kent-academic-repository#policies) (available from <https://www.kent.ac.uk/guides/kar-the-kent-academic-repository#policies>).

The survivability of phyllosilicates and carbonates impacting Stardust Al foils: Facilitating the search for cometary water

Penelope J. WOZNIAKIEWICZ^{1,2*}, Hope A. ISHII³, Anton T. KEARSLEY^{1,2}, John P. BRADLEY³,
Mark. C. PRICE¹, Mark J. BURCHELL¹, Nick TESLICH⁴, and Mike J. COLE¹

¹School of Physical Science, Centre for Astrophysics and Planetary Sciences, University of Kent, Canterbury CT2 7NH, UK

²Department of Earth Sciences, Impacts & Astromaterials Research Centre (IARC), Natural History Museum,
London SW7 5BD, UK

³Hawai'i Institute of Geophysics and Planetology, University of Hawai'i at Mānoa, 1680 East-West Road, POST 602,
Honolulu, Hawai'i 96822, USA

⁴Lawrence Livermore National Laboratory, 7000 East Avenue, Livermore, California 94550, USA

*Corresponding author: E-mail: pjw@kent.ac.uk

(Received 22 May 2015; revision accepted 28 September 2015)

Abstract—Comet 81P/Wild 2 samples returned by NASA's Stardust mission provide an unequalled opportunity to study the contents of, and hence conditions and processes operating on, comets. They can potentially validate contentious interpretations of cometary infrared spectra and in situ mass spectrometry data: specifically the identification of phyllosilicates and carbonates. However, Wild 2 dust was collected via impact into capture media at $\sim 6 \text{ km s}^{-1}$, leading to uncertainty as to whether these minerals were captured intact, and, if subjected to alteration, whether they remain recognizable. We simulated Stardust Al foil capture conditions using a two-stage light-gas gun, and directly compared transmission electron microscope analyses of pre- and postimpact samples to investigate survivability of lizardite and cronstedtite (phyllosilicates) and calcite (carbonate). We find the phyllosilicates do not survive impact as intact crystalline materials but as moderately to highly vesiculated amorphous residues lining resultant impact craters, whose bulk cation to Si ratios remain close to that of the impacting grain. Closer inspection reveals variation in these elements on a submicron scale, where impact-induced melting accompanied by reducing conditions (due to the production of oxygen scavenging molten Al from the target foils) has resulted in the production of native silicon and Fe- and Fe-Si-rich phases. In contrast, large areas of crystalline calcite are preserved within the calcite residue, with smaller regions of vesiculated, Al-bearing calcic glass. Unambiguous identification of calcite impactors on Stardust Al foil is therefore possible, while phyllosilicate impactors may be inferred from vesiculated residues with appropriate bulk cation to Si ratios. Finally, we demonstrate that the characteristic textures and elemental distributions identifying phyllosilicates and carbonates by transmission electron microscopy can also be observed by state-of-the-art scanning electron microscopy providing rapid, nondestructive initial mineral identifications in Stardust residues.

INTRODUCTION

Comets are frozen objects that have remained largely undisturbed since their accretion in the cold outer regions of the early solar system (Brownlee 2003). It is therefore believed that their mineralogy and their structure (on nanometer to kilometer scales) should

retain evidence of the conditions and processes operating in the early solar system. For decades, the composition of cometary dust has been investigated by astronomical observations in the infrared (e.g., Maas et al. 1970; Hanner et al. 1994; Crovisier et al. 1997). The $\sim 10 \mu\text{m}$ and $\sim 16\text{--}35 \mu\text{m}$ spectral features have often been attributed to amorphous and crystalline silicates, a

conclusion consistent with the supposedly unperturbed nature of comets, and showing preservation of pristine samples of materials accreted in the comet-forming region: Crystalline silicates would represent samples of inner nebula materials transported to the comet-forming region while amorphous silicates might represent remnants of the collapsing presolar molecular cloud. However, Spitzer Space Telescope infrared spectra obtained from comet 9P/Tempel 1 after the Deep Impact event (where a passing spacecraft observed the impact of a separate probe into a comet nucleus) give a “best fit” to combined spectra of reference materials if carbonates (5% by surface area of all dust detected) and phyllosilicates (8% by surface area of all silicates) are included (Lisse et al. 2006). Possible cometary carbonates had also been discussed by Fomenkova et al. (1992) who inferred their signature in mass spectrometry data from the VEGA 1 and 2 spacecraft encounter with comet 1P/Halley. To this day, these identifications remain controversial, especially as the parageneses of most carbonate and phyllosilicate minerals are commonly believed to require aqueous processes (Deer et al. 1992). Prolonged presence of liquid water on a cometary parent body would certainly challenge the common conception of these icy objects as having remained frozen since accretion very early in the history of the solar system. Whether phyllosilicates (and carbonates) could eventually form in a mixture of micrometer-scale anhydrous silicate dust and ices, during brief but intense shock heating associated with hypervelocity impact processes on a cratered comet surface is currently unknown. However, could this paradox be explained by emerging alternative formation mechanisms? For example, Toppani et al. (2005) have demonstrated that carbonates may form during nonequilibrium condensation of a silicate glass in H₂O-CO₂-rich vapor environments, and Ciesla et al. (2003) have proposed that fine-grained (<100 nm) phyllosilicates may form through rapid mineral hydration as a result of shockwaves in icy regions of the nebula. Perhaps we should momentarily set aside a prior contention that all comets are the most primitive of bodies, and consider the implications of the assemblage of minerals already observed in comet 81P/Wild 2. The presence of refractory minerals and chondrule fragments in the Stardust collection (e.g., Joswiak et al. 2012) has shown that there was substantial early migration of impact-comminuted, partially equilibrated chondritic material out to the comet-forming region. The recognized assemblage of sulfide minerals (e.g., Zolensky et al. 2008; Berger et al. 2011) would be consistent with a source from a body upon which aqueous processes had been important. If carbonates and phyllosilicates pre-date accretion of the

cometary body, could they too even have come from earlier disaggregation of substantial asteroidal bodies, similar to those which today yield the CR, CM, and CI carbonaceous chondrite meteorites? This would imply that at least some comets are relatively late-formed by comparison to the asteroids (and even planets). It is clear that we need to know if these minerals really are present within comets.

Unfortunately, interpretation of astronomical infrared spectral data is problematic, with properties such as the temperature, size, and shape of the absorbing/emitting grains influencing the strength and position of different characteristic peaks (see e.g., Hanner et al. 1994; Henning and Mutschke 1997; Min et al. 2008). It is therefore necessary to confirm the presence of phyllosilicates and carbonates in samples of comets available for study in the laboratory.

Interplanetary dust particles (IDPs) are small particles (typically less than 100 μm in diameter) of extraterrestrial dust collected in the stratosphere by high altitude aircraft. The exact parent body from which each individual IDP originates is, at best, uncertain. However, it is generally considered that the chondritic porous subtype (CP IDPs) are cometary in origin: their fine-grained, fragile aggregate nature are consistent with observations that cometary meteors readily disaggregate (Verniani 1969); the high speeds at which some enter the atmosphere (as determined from He release profiles) is consistent with capture from cometary orbits (Brownlee et al. 1993, 1994, 1995); the silicate features in infrared spectra obtained from CP IDPs in the laboratory are similar to those observed in the astronomical spectra of comets (Sandford and Walker 1985; Bradley et al. 1999; Molster and Waters 2003); and their unequilibrated, anhydrous mineralogies, combined with the high content of presolar grain and carbonaceous material, suggest they have not been subjected to significant processing on the parent body, which is consistent with our understanding of cometary evolution (Bradley 2003, 2013). In contrast, the chondritic smooth (CS) IDPs are low-porosity particles composed primarily of hydrated layer silicates, with lesser anhydrous crystalline and amorphous silicates; sulfides (predominantly Ni-rich); and in some cases, carbonates (see Bradley 2003, 2013 for reviews). These CS IDPs share several mineralogical and petrographic similarities with fine-grained matrices of some carbonaceous meteorites and they are generally believed to originate from asteroids. However, the distinction between cometary and asteroidal origins is heavily based on the presence or absence of hydrated minerals, with the pre-existing assumption that the parent body processes required for hydrated mineral formation (aqueous alteration) occur on asteroids but not on comets. To obtain an unbiased view of the

contents of comets, we must therefore look to cometary samples with known origins.

The return of samples from comet 81P/Wild 2 by NASA's Stardust mission provides an unequalled opportunity for unambiguous and unbiased laboratory analyses of "fresh" cometary dust and comparisons against the spectral data and IDPs and meteorites already in our collections. The Stardust spacecraft flew through the comet's coma and captured grains leaving the comet's nucleus in the aerogel cells and Al foil surfaces of its collector. Phyllosilicates have yet to be found in the aerogel of the Stardust collector (Zolensky et al. 2006, 2008). In contrast, carbonates have been positively identified in several Stardust aerogel samples (e.g., Wirick et al. 2007; Flynn et al. 2008); however, these authors have recognized concerns over premission purity and postmission contamination of the aerogel, calling into question the cometary origin of these grains. Confirmation of cometary carbonates in Wild 2 should therefore be provided by their identification within an indisputable impact feature on Stardust Al foils, whose composition and structure is well known (Kearsley et al. 2007) and does not contain material likely to be confused with these minerals. To date, however, neither carbonates nor phyllosilicates *of cometary origin* have been positively identified on the Stardust foil. However, it is important to remember that grains were captured as they impacted into the Stardust collection media at $\sim 6 \text{ km s}^{-1}$ (Brownlee et al. 2003, 2006). Impacting particles experienced high pressures and temperatures as they came to a halt along or at the end of the tracks they carved out in aerogel, or as they formed residues covering the floors of the craters they excavated in foil. Previous experimental work has studied the effect of such capture on a variety of anhydrous silicates and metal sulfides, finding that the high pressures and temperatures generated during the impacts can result in varying degrees of alteration—from fracturing to melting to vaporization (e.g., Ishii et al. 2008; Wozniakiewicz et al. 2011, 2012a, 2012b). Burchell et al. (2006) and Noguchi et al. (2007) have also demonstrated that some portion of large (150 μm) phyllosilicate grains can survive impact into the collector's aerogel cells with intact layered structures and compositions; however, these grains are toward the maximum grain size collected by Stardust (Hörz et al. 2006; Kearsley et al. 2008). Although the Al foils were not pure in composition, and impacting particles are subjected to higher peak pressures (typically 60–90 GPa in impacts on foils, Burchell and Kearsley 2009; compared to 800 MPa during capture in aerogel, Trigo-Rodríguez et al. 2008), the foil collection medium has been noted as potentially superior to the aerogel in several ways: Foils capture the impacting grains within a relatively confined

volume (i.e., within a crater rather than at the end of, and along, a track); they have comparatively high thermal conductivity, ensuring the heat generated during impact is transferred away quickly; they have a silicon-poor composition such that the identification of most rock-forming minerals may still be possible by examining major element to Si ratios; and the craters formed by impacting particles are often easier to find compared to the tracks generated by impacts into aerogel, particularly at the smaller size scales (see Wozniakiewicz et al. [2012a] for a more complete discussion). However, it remains unknown in what manner phyllosilicates, or carbonates, are modified by impact with the Stardust Al foils. There are reasons for supposing that these volatile-bearing minerals behave differently to those minerals that do not contain volatiles. Burchell et al. (2008a) for example, report that while the nonvolatile-bearing minerals olivine, enstatite, diopside, and wollastonite readily give Raman spectra from crater residues after impact in Al foil at $\sim 6 \text{ km s}^{-1}$, the phyllosilicate lizardite does not. To provide clear diagnostic criteria for future work on Stardust materials, and to be confident that what we have so far interpreted as apparent absence is not simply failure to recognize the remains of two important components, we need to understand how these minerals may be modified by collection, and hence whether they could be positively identified within Stardust collections.

To investigate the survivability of phyllosilicates and carbonates, we have undertaken a series of laboratory experiments, impacting well-characterized samples of these minerals into Al foils to simulate their capture in the Stardust collector. By analyzing and directly comparing the original projectiles and resulting residue samples, we are able to determine whether these materials have been preserved and, if not, how they have been modified. The experiments and results from our mineralogical analyses are described in this paper.

SAMPLES AND METHODOLOGY

Impact Analogue Sample Production

The phyllosilicate and carbonate impact analogue foils were generated using the two-stage light-gas gun (LGG) in the Centre for Astrophysics and Planetary Sciences at the University of Kent, Canterbury (Fig. 1A). This facility has been used extensively to simulate the Stardust capture conditions by accelerating and impacting chosen projectiles to $\sim 6 \text{ km s}^{-1}$ into Stardust analogue targets (e.g., Kearsley et al. 2006, 2007, 2008, 2009; Burchell et al. 2008a, 2008b; Wozniakiewicz et al. 2009, 2011, 2012a, 2012b; Price et al. 2010; Floss et al. 2013; Croat et al. 2015).

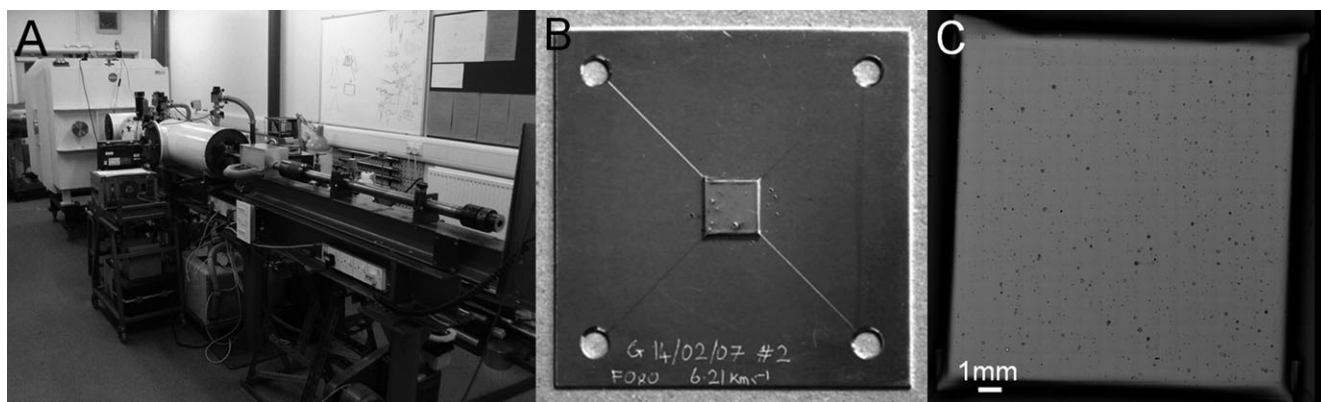


Fig. 1. Impact analogue sample production. A) The two-stage light-gas gun (LGG) at the University of Kent. B) Photograph of an analogue foil wrapped around metal blank and mounted on metal plate, after shooting. C) Backscattered electron (BSE) image montage of an impacted foil target.

For the studies detailed in this paper, the projectiles (also referred to as impactors) were samples of the phyllosilicate minerals lizardite ($\text{Mg}_3\text{Si}_2\text{O}_5(\text{OH})_4$) and cronstedtite ($\text{Fe}^{2+}_2\text{Fe}^{3+}(\text{Si},\text{Fe}^{3+})_2\text{O}_5(\text{OH})_4$) and the carbonate mineral calcite (CaCO_3). These were from collections at the Natural History Museum, London (NHM): lizardite—BM.43217; cronstedtite—currently awaiting cataloging; calcite—BM.2005, M315. To ensure the production of craters within the range of sizes observed in Stardust Al foils, we prepared phyllosilicate and carbonate projectiles by crushing with a ceramic pestle and mortar. The most numerous craters identified during the Stardust preliminary examination (PE) had been less than $20\ \mu\text{m}$ in diameter and produced by cometary particles $<6.5\ \mu\text{m}$ in diameter, based on the particle–crater diameter correlations of Kearsley et al. (2006) and Price et al. (2010). However, the great majority of the cometary dust mass in the Stardust foils lies within craters larger than $20\ \mu\text{m}$ in diameter (Kearsley et al. 2008; Price et al. 2010). Sixty-three such craters were identified during the PE, the largest measuring $680\ \mu\text{m}$ in diameter and resulting from the impact of a cometary particle estimated to measure $\sim 150\ \mu\text{m}$. To restrict experimental craters to the major part of the range of crater sizes observed on Stardust, powdered grains were passed through a $53\ \mu\text{m}$ sieve to remove coarser grains from the projectile sample and thus prevent these larger grains dominating our data. Given the size calibrations mentioned above, we thus expected the largest craters from single grains to be of order $250\ \mu\text{m}$ in diameter.

The target used in each case was a sample of flight-spares Stardust Al foil (provided by F. Hörz of NASA JSC). Details of this foil can be found in Kearsley et al. (2007). For the experimental light-gas gun shots, the foil was wrapped around a $1\ \text{mm}$ thick square Al alloy plate measuring $\sim 1.5\ \text{cm} \times 1.5\ \text{cm}$, to simulate the

mounting on the Stardust collector. To facilitate handling during later analyses, these targets were held with conductive adhesive putty onto an Al base-plate (Fig. 1B). Throughout this preparation procedure, gloves and pliers were used to avoid contamination of the foil.

The light-gas gun set-up and velocity measurement techniques employed here are described in Burchell et al. (1999). In each shot the target chamber was evacuated to a few $\times 10^{-1}$ mbar, or less, to minimize velocity loss in flight. All projectiles consisted of powders of a single mineral, generating separate impact analogue foils (e.g., Fig. 1C) to ensure any identifications made were associated with the correct mineral. Details of these shots are provided in Table 1.

Analytical Instrumentation and Sample Preparation and Analysis

A large array of analytical tools are currently available for mineral analyses (e.g., Zolensky et al. 2000 and references therein). Scanning electron microscopy (SEM) with energy dispersive X-ray microanalysis (EDX) is a widely available technique used extensively to image and perform initial compositional analyses of residues in craters on the Stardust Al foils (e.g., Zolensky et al. 2006; Kearsley et al. 2008). Accordingly, SEM was used to perform initial “rough” imaging of the impacted foils and locate craters $>50\ \mu\text{m}$ in diameter for further study by transmission electron microscopy (TEM). Although each mineral projectile was shot separately at different targets, it is still possible for gun-derived debris to be accelerated and impact the targets generating craters that, in terms of their morphology, are indistinguishable from those of the intended projectiles (see Wozniakiewicz et al. 2009). SEM EDX was therefore used to identify those craters

Table 1. Details of projectiles and parameters for two-stage light-gas gun (LGG) shots studied in this paper.

Shot	Projectiles (NHM sample)	Projectile size (μm)	Impact speed (km s^{-1}) \pm 2%
G110507#4	Lizardite (BM.43217)	<53	5.99
G010606#3	Cronstedtite (uncataloged)	<53	5.58
G010507#2	Calcite (BM.2005,M315,)	<53	5.77

with residues exhibiting spectra containing the major elements of the intended impactors: It has been shown that SEM EDX can provide a useful initial identification of the precursor mineral (e.g., Kearsley et al. 2007, 2008; Wozniakiewicz et al. 2009, 2011). The initial SEM imaging and EDX analyses for this investigation were conducted using the JEOL JSM-7401F SEM at Lawrence Livermore National Laboratory (LLNL). EDX microanalyses were obtained through an Oxford Instruments system, running INCA software (version 18). Additional SEM imaging and EDX analysis was performed using the FEI Quanta 650 FEG SEM at the NHM which is equipped with an annular, multisegment Bruker XFlash FlatQUAD Silicon Drift Detector (SDD) for EDX analyses.

Once suitable craters were identified, TEM was used to perform more in-depth analyses of the preimpact projectiles and postimpact crater residues to identify those features generated by the impact and those inherent to the impactor. TEM is a technique capable of high resolution compositional and structural analyses required for mineralogical classifications over the small scales applicable to the projectiles and crater residues. Focused ion beam (FIB) microscopy was required to prepare electron transparent thin sections for TEM from the bulk specimens; however, this was complicated by the topographies of our craters, which made lift-out of the sections impossible. Therefore, the shot foil specimens were first mounted vertically within a resin block and polished down until the cross section of the craters (and their residues) were exposed for FIB. Projectile materials were similarly embedded in resin blocks prior to FIB preparation. For more details of sample preparation for FIB, see Wozniakiewicz et al. (2011). The FIB sections were then produced using the FEI Nova600 NanoLab dual-beam FIB microscope at LLNL.

The FIB-prepared sections were then analyzed using the FEI Titan G2 80–300 kV dual-aberration-corrected and monochromated scanning TEM (STEM) at LLNL. The Titan is equipped with a high angle annular dark field (HAADF) Si(Li) solid-state energy dispersive X-ray spectrometer. Data were collected at 300 kV. All

samples were first imaged in TEM bright and dark field and STEM HAADF modes. Electron diffraction patterns and EDX spectra were obtained from the projectile sections to confirm homogeneity, initial crystallinity, and composition. For the highly complex residue sections, diffraction patterns were collected to confirm the identity of amorphous and crystalline components, and TEM EDX data and STEM EDX mapping provided accompanying chemical data. TEM EDX atom% data was obtained using ES Vision software (v. 4.1).

RESULTS AND DISCUSSION

Bright field TEM images of each projectile and residue section are shown in Figs. 2 and 3. Our TEM analyses confirm that the phyllosilicate projectiles used in this study are pure, crystalline samples of lizardite and cronstedtite: Representative indexed diffraction patterns are shown in Fig. 2 and chemical data are plotted on Figs. 4 and 5 (these data cluster over the location of their theoretical compositions). For the calcite projectile, diffraction data was also consistent with crystalline calcite (Fig. 2). The chemical data are also clustered; however, the relative proportions of C, O, and Ca are inconsistent with the theoretical composition for calcite. Elemental abundances for low compared to higher Z elements (e.g., C and O compared to Ca), can depart from true values due to different self-absorption of X-rays within the FIB section thickness. Consequently, Cliff-Lorimer k-factors were independently calculated from the well-characterized NHM calcite projectile and a manual correction applied. Since the NHM calcite diffraction data are consistent with crystalline calcite, and since we are performing a direct comparison between pre- and postimpact samples that have been prepared using the same FIB preparation (approximately the same thickness), the projectile section is appropriate as the standard for corrections to the residue EDX data to obtain relative element abundances (detailed below in the Calcite section and displayed in Fig. 6). As a consequence, the abundances of only those elements present in the projectile (Ca, C, and O) are quantified and plotted in Fig. 6.

The residue sections are complex, exhibiting varied effects of impact for each mineral. These are discussed in turn below.

Lizardite

The lizardite residue is highly vesiculated (Fig. 7), a texture indicative of the release of volatiles (in this case, OH) from a melt generated during the intense impact-

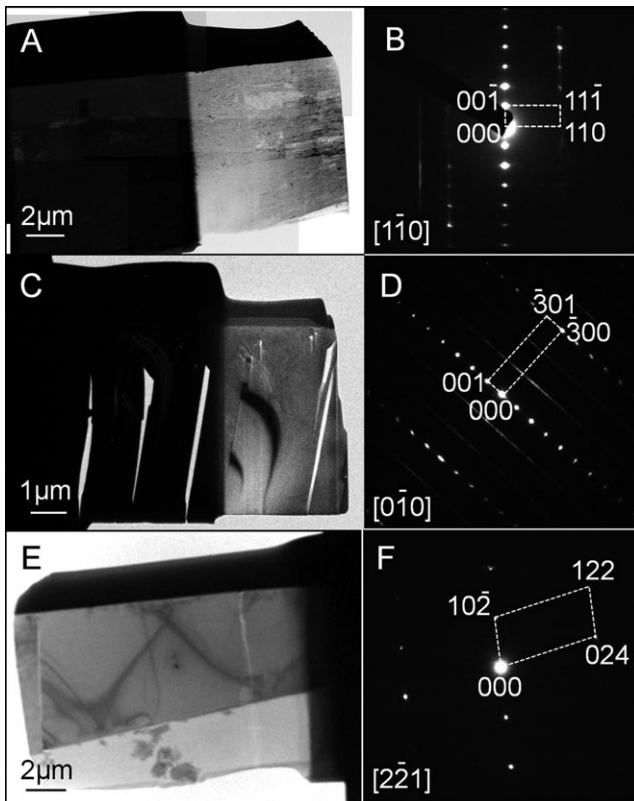


Fig. 2. Bright field TEM images and representative selected area electron diffraction patterns for the preimpact projectiles lizardite (A, B), cronstedtite (C, D), and calcite (E, F).

generated heating. Dark field STEM imaging combined with diffraction patterns show the residue to be completely amorphous. The presence of C in some of our TEM EDX analyses over vesiculated regions of the lizardite residue indicates that resin was able to permeate the residue during preparation (embedding) for FIB work. A correction was therefore applied to remove the contribution of O from the resin based on analyses of nearby resin in the section. The corrected EDX data for the lizardite residue were used to plot Fig. 4. The data indicate that the lizardite residue retains a Mg to Si ratio close to that of the original impactor, although slightly depleted in Mg: $100\text{Mg}/(\text{Mg}+\text{Si}) = 55.0 \pm 2.8$ (1σ error) in the residue compared to 60.1 ± 1.1 in the original projectile. The section thickness is nonuniform due to complexities of FIB-milling heterogeneous residues, as well as the vesiculated nature of the residue and, as such, the slightly lower Mg counts observed for the residue data may be due to greater X-ray absorption for low-Z elements in thicker regions. Minor loss of Mg cannot be completely excluded although previous work suggests Si would be preferentially lost: the evaporation experiments of Hashimoto (1983) reveal the higher

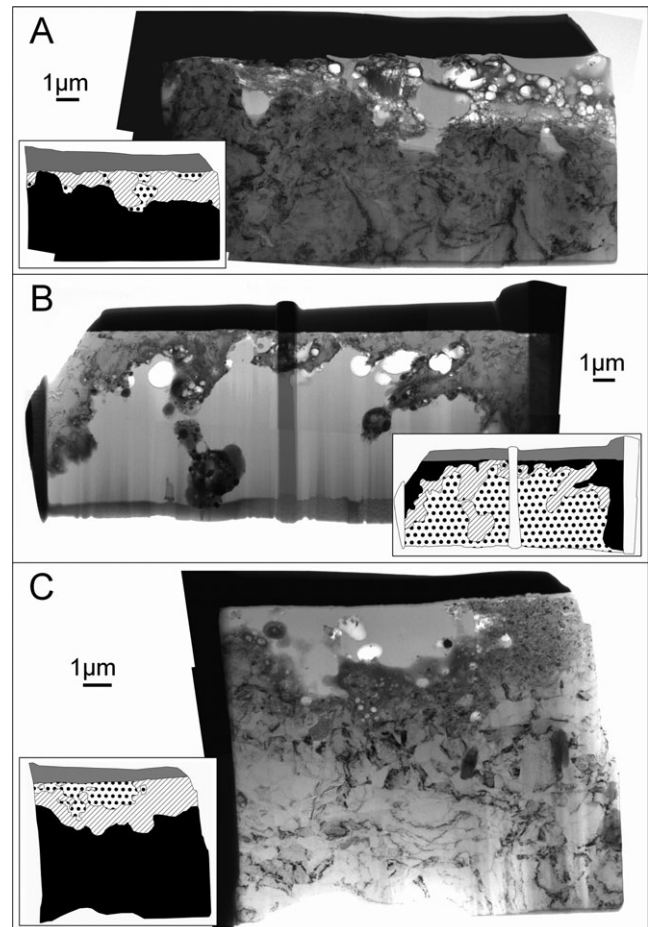


Fig. 3. Bright field TEM images of lizardite (A), cronstedtite (B), and calcite (C) residue sections with inset illustration identifying the Al foil (black), protective Pt strap from the FIB extraction process (gray), embedding resin (spotted), and the residue (striped).

volatility of SiO_2 compared to MgO , and the laser heating experiments of Gerasimov et al. (2000) show the initial preferential loss of Si over Mg from glasses (this reverses as vaporization continues). We note, however, that the peak temperature durations applicable to their experiments were much longer than those applicable to Stardust impacts: peak temperatures were sustained for $\sim 10^{-3}$ s during the laser heating experiments of Gerasimov et al. (2000) and on the order of minutes to hours during the evaporation experiments of Hashimoto (1983), whereas for Stardust impacts we estimate the duration of heating is on the order of 10^{-9} s assuming the duration of contact and compression stage is roughly equal to the time taken for the projectile to traverse its own diameter (see Melosh 1989). The $(\text{Mg}+\text{Si})$ to O ratio of the residue also remains close to that of the original projectile with minor loss of O relative to Mg and Si: $100(\text{Mg}+\text{Si})/(\text{Mg}+\text{Si}+\text{O}) =$

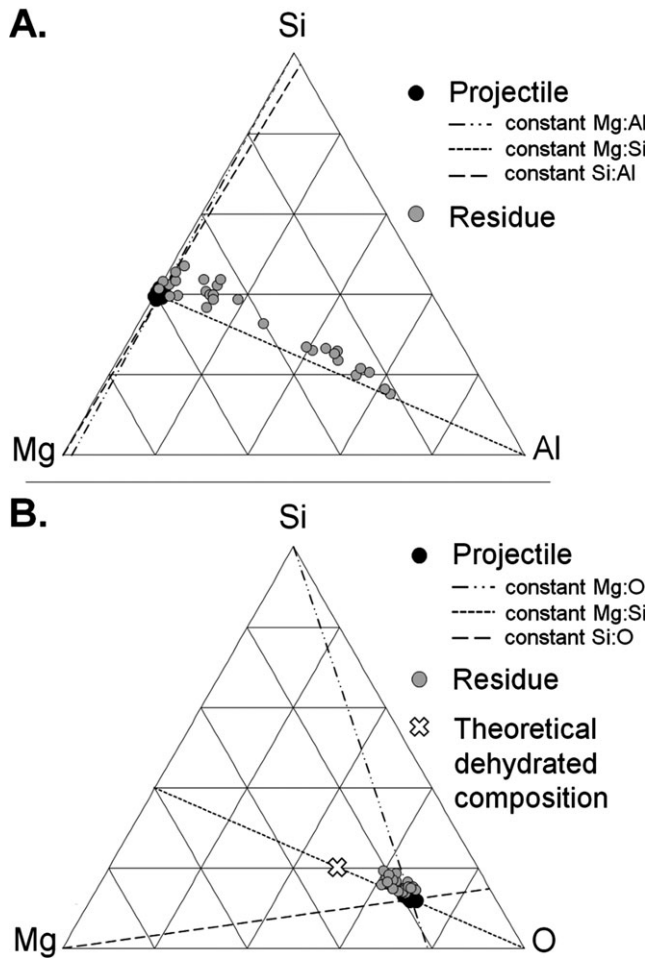
LIZARDITE

Fig. 4. Ternary diagrams displaying relative abundances of (A) Mg:Si:Al and (B) Mg:Si:O based on atom% data from the TEM EDX analyses of lizardite preimpact projectile (12 data points—solid black circles) and postimpact residue (29 data points—gray circles). Theoretical composition of dehydrated lizardite (having lost OH) is also plotted (white cross).

35.5 ± 2.5 (1σ error) from 30.5 ± 1.1 . Again, nonuniform section thickness may result in varied X-ray absorption and lower O counts from thicker regions. However, volatile components like water are expected to be released from molten residue upon impact (e.g., Langenhorst 2002). A composition representative of fully dehydrated lizardite (having lost OH) is marked on Fig. 4B (cross at $100\text{Mg}/[\text{Mg}+\text{Si}] = 60$ and $100[\text{Mg}+\text{Si}]/[\text{Mg}+\text{Si}+\text{O}] = 50$). We note that despite the presence of abundant vesicles indicative of volatile release throughout the residue, it appears that at least some O has been retained. Al has become incorporated into the silicate melt (Fig. 4A), and it may therefore be that metal oxidation has retained O within the residue. EDX maps obtained over an area of this residue are shown in

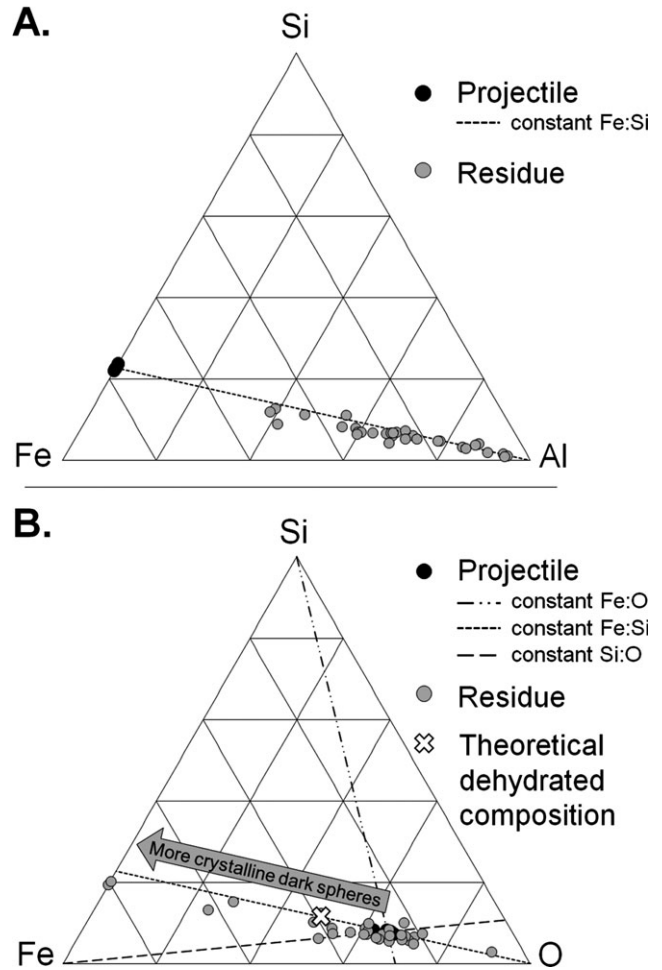
CRONSTEDTITE

Fig. 5. Ternary diagrams displaying relative abundances of (A) Fe:Si:Al and (B) Fe:Si:O based on atom% data from the TEM EDX analyses of the cronstedtite preimpact projectile (7 data points—solid black circles) and postimpact residue (31 data points—gray circles). Theoretical composition of dehydrated cronstedtite (having lost OH) is also plotted (white cross).

Fig. 8. Although the variations in elemental ratios are difficult to interpret due to the varied thickness of residue where vesiculated, the Si maps exhibit several discrete <50 nm Si hot spots (highlighted in Fig. 9). Core loss electron energy loss spectra taken over these areas (Fig. 9) exhibit a minor peak at ~ 101 eV as well as the two adjacent peaks at ~ 108 eV and ~ 116 eV, consistent with the presence of native silicon (Si^0) among the silicate glass (compared against Si-L edge positions reported in Batson 1991). Although the Si-L edge position for SiC (also at ~ 101 eV, see Schneider et al. 1996) would be indistinguishable from Si^0 given the level of noise, the absence of C hot spots in the location of the beads (see Fig. 11) suggests that they are

CALCITE

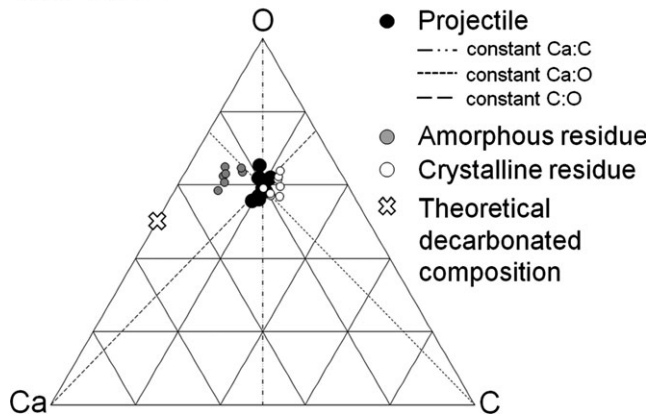


Fig. 6. Ternary diagram displaying relative abundances of Ca:C:O based on atom% data from the TEM EDX analyses of the calcite preimpact projectile (12 data points—solid black circles) and STEM EDX analyses of the postimpact residue (15 data points—hollow circles for crystalline residue and gray circles for amorphous residue). Theoretical composition of decarbonated calcite (having lost CO_2) is also plotted (white cross).

native silicon rather than SiC . During the collection of these data, these features appeared to homogenize with the surrounding melt, such that additional spectra exhibited only the SiO_2 peaks. Native silicon is rare in planetary materials. On Earth, the best documented occurrence of native silicon has been in a fossilized lightning strike known as a fulgurite (e.g., Essene and Fisher 1986), where the sudden high temperatures resulted in melting and it is believed that the presence of organic carbon (from soils and plant roots) led to the reduction of silicon (this produced not only native silicon but also Fe-silicides—see discussion in the Cronstedtite section). Native silicon has also more recently been identified in the lunar meteorite Dhofar 280 (e.g., Nazarov et al. 2012, 2015) and fragments of lunar regolith returned by Apollo 16 (Spicuzza et al. 2011), where they are thought to result from condensation of impact-induced vapor, with reduced conditions promoted by the fractionation of SiO and oxygen in the expanding impact vapor cloud. An impact-induced origin for these extraterrestrial samples is supported by their identification in our impact residues as well as within the silicate impact melts studied previously by Fiske et al. (1995). However, in the experimental melts, we propose that the reducing conditions may have been produced by the materials involved: in the case of our Stardust lizardite impact analogues, we believe the Al foil target melted upon impact, forming an O-scavenging melt that incorporated O from released water vapor and also combined with, and in some locations reduced, the remaining projectile

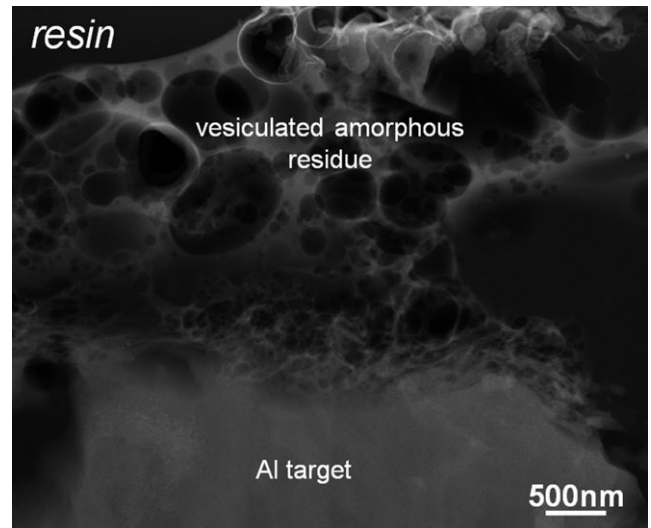


Fig. 7. HAADF STEM image of a region of the lizardite residue showing the highly vesiculated texture resulting from hypervelocity impact.

melt. Upon impact, the lizardite has therefore been subjected to melting, release of volatiles, incorporation (and oxidation) of Al, and formation of <50 nm native silicon beads before solidifying as an amorphous, vesiculated residue. Although the results suggest that the whole impacting grain was subjected to melting, we cannot discount the possibility that surviving lizardite may exist elsewhere in these craters, in locations not sampled by this FIB-generated TEM section.

Cronstedtite

The cronstedtite residue is also vesiculated indicating the release of volatiles upon melting, although to a lesser degree than the lizardite. As with the lizardite, the presence of carbon in some of our TEM EDX analyses over vesiculated regions of the cronstedtite residue indicates that resin was able to permeate the residue during preparation for FIB. A similar correction was therefore applied to remove the contribution of O from the resin, and these corrected EDX data were used to plot Fig. 5. Dark field STEM imaging, combined with diffraction patterns, show that the bulk of the residue is amorphous; however, there are a large number of submicron crystalline spheres present throughout (seen in Fig. 10). The EDX spectra and maps obtained over an area of the cronstedtite residue (Figs. 5 and 11) show the amorphous residue to be an Fe- and Al-bearing silicate glass. The cronstedtite residue, like the lizardite residue, has thus incorporated Al from the target during impact. The submicron crystalline spheres within the amorphous residue are Fe-

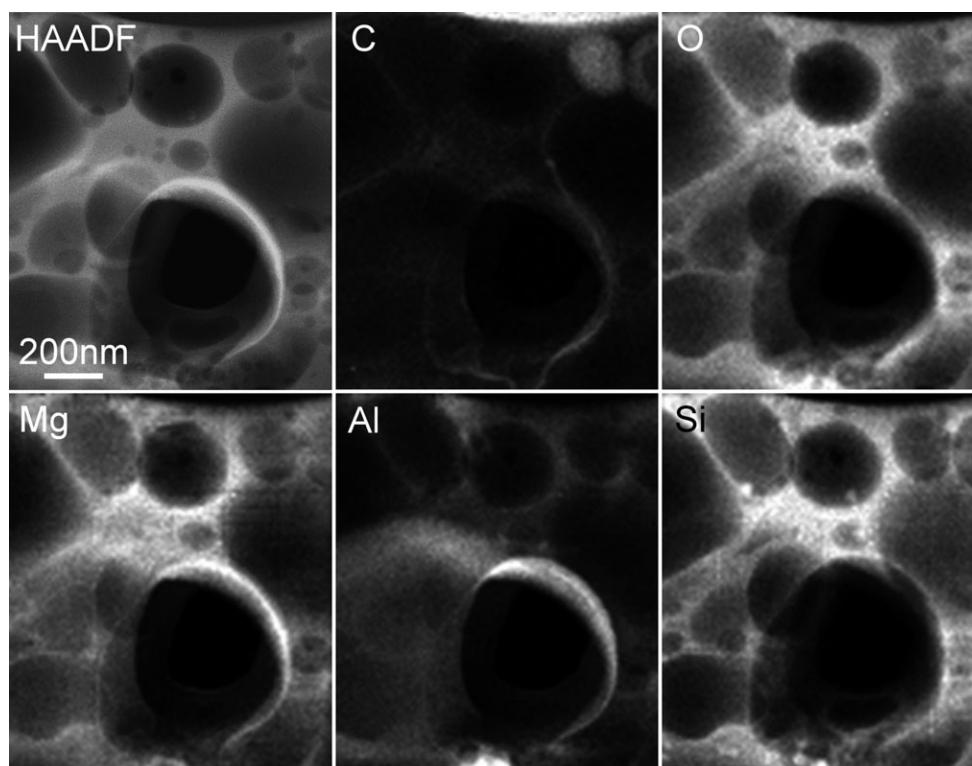


Fig. 8. Elemental abundance maps from $K\alpha$ X-rays of C, O, Mg, Al, and Si taken over a region of the lizardite residue section by STEM EDX mapping. Top left panel is the HAADF STEM image of this region.

rich. The Al foil contains randomly distributed, pre-existing, Fe-rich inclusions (Kearsley et al. 2007) which, if impacted, might spread Fe melt droplets throughout a residue; however, the EDX data indicate the bulk Fe to Si ratio of the residue has remained close to that of the original projectile (Fig. 5, $100\text{Fe}/[\text{Fe}+\text{Si}] = 79.1 \pm 4.0$ [1σ error] from 77.3 ± 0.8 originally). This suggests that Fe has not been added, but instead, that these spheres are the result of segregation of Fe from the cronstedtite projectile. Indeed, magnetite spheres have been observed in the amorphous rims of cronstedtite grains recovered after impact into silica aerogel (Noguchi et al. 2007). On closer inspection of the EDX maps (Fig. 11) we note that some of the Fe-rich beads also appear rich in Si suggesting they are Fe-silicide beads. Fe-silicides are rare in planetary materials. Like native silicon, they are found in fulgurites (e.g., Essene and Fisher 1986), and have been identified in the lunar meteorite Dhofar 280 (Anand et al. 2004; Nazarov et al. 2012) and Apollo 16 lunar regolith fragments (Spicuzza et al. 2011). They have also been identified in several ureilite meteorites (e.g., Keil et al. 1982; Herrin et al. 2008; Ross et al. 2009; Smith et al. 2010). Fe-silicide beads similar in size to those we observe in the cronstedtite residue (<100 nm) have also previously been identified near the entrance of track #44 in the

Stardust aerogel cell C2004 (Rietmeijer et al. 2008). It is generally believed that those observed in the ureilite and lunar samples were produced during impacts occurring on the parent body (although for ureilites it has also been suggested they may instead represent samples of the parent body core, e.g., Ross et al. 2009; Smith et al. 2010). Those identified in Stardust aerogel are also believed to result from impacts, although they are instead believed to have formed as a result of the particle collection method (i.e., via impact) rather than as a result of impacts on the parent body. Indeed, Fe-silicide beads of a range of Si-contents have previously been identified in melts produced during shock experiments: Badjukov and Petrova (1991) identified Fe-silicides in melts produced by a range of silicate targets shocked in cylindrical steel containers surrounded by high explosive and Rowan and Ahrens (1994) observed them in the experimental impact melts produced in samples of midocean ridge basalts. The Fe-silicide phases are thought to have formed as a result of melting and mixing of Fe and Si (from the materials involved) under reducing conditions. The reducing conditions in each case are thought to be produced by the materials involved: e.g., in the case of Stardust, it was suggested that carbonaceous material in the impacting cometary grain and/or the aerogel itself may

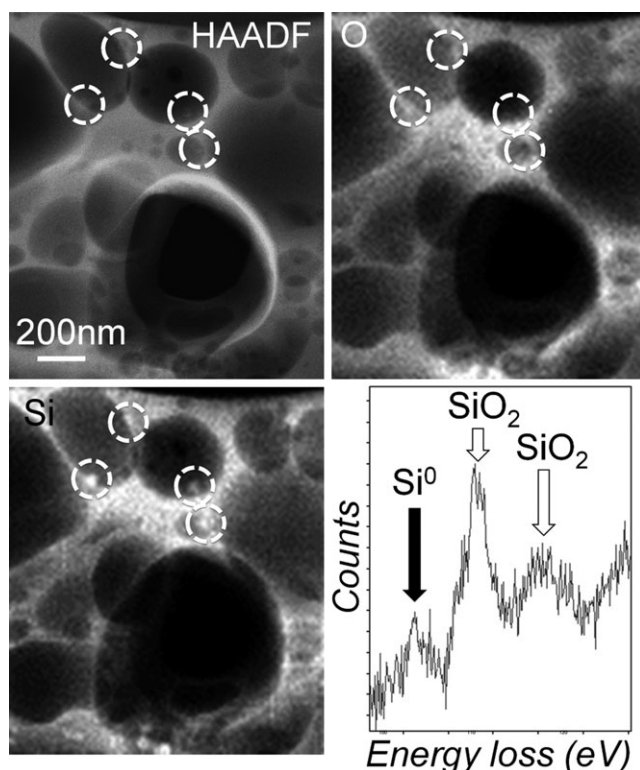


Fig. 9. Reduced silicon (Si^0) beads observed in the lizardite residue. Locations of these beads are highlighted by dashed white circles in the HAADF image (top left), O map (top right), and Si map (bottom left). An example of a core loss electron energy loss spectrum taken over one of these beads (bottom right) shows the presence of a minor peak at ~ 101 eV as well as the two adjacent peaks at ~ 108 eV and ~ 116 eV consistent with the presence of reduced silicon (Si^0) among the silicate glass.

have decreased oxygen fugacity in the melted material, thus promoting the reduction of silicates (Rietmeijer et al. 2008). In the case of our cronstedtite impacts into Al foils, the reducing conditions may have been produced by the Al foil target, which upon impact formed an O-scavenging melt.

The average (Fe+Si):O ratio of the residue has increased, indicating a loss of O during impact: $100 (\text{Fe}+\text{Si})/(\text{Fe}+\text{Si}+\text{O}) = 42.5 \pm 19.7$ (1σ error) for the residue compared to 34.5 ± 1.6 for the original projectile. As with the lizardite, however, the bulk composition is not consistent with a completely dehydrated cronstedtite (having lost OH), where $100 (\text{Fe}+\text{Si})/(\text{Fe}+\text{Si}+\text{O}) = 50$ (as marked on Fig. 5B). It therefore again appears that the production of molten O-scavenging Al has resulted in the retention of some of the impact-liberated O. Upon impact, cronstedtite has therefore been subjected to melting, release of volatiles, incorporation (and oxidation) of Al and formation (by reduction) of crystalline Fe and Fe-Si-rich beads, before

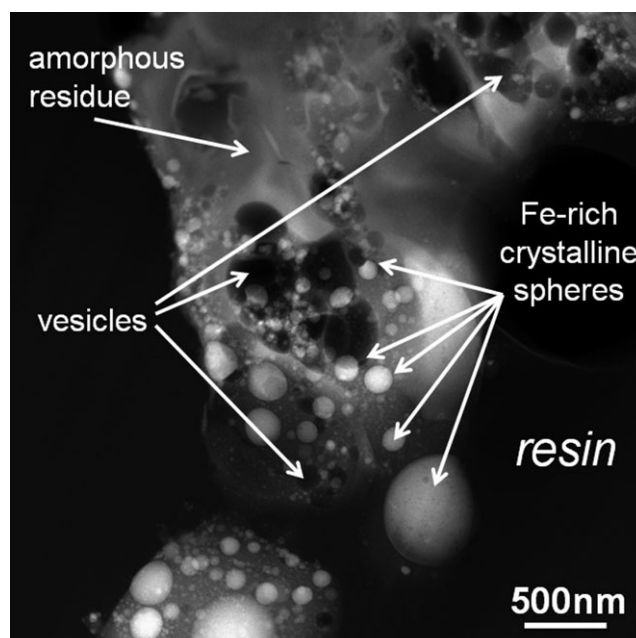


Fig 10. HAADF STEM image of a region of the cronstedtite residue. The residue is amorphous and moderately vesiculated and exhibits discrete crystalline Fe- and Fe-Si-rich beads (typically < 500 nm) throughout.

solidifying as a largely amorphous, vesiculated residue. Although the results suggest that the whole impacting grain was subjected to melting, we cannot discount the possibility, as with the lizardite, that surviving cronstedtite may exist elsewhere in these craters, in locations not sampled by this FIB-generated TEM section.

Calcite

The calcite residue is a mixture of crystalline and vesiculated amorphous material, the former being polycrystalline with individual crystals < 100 nm in scale (see Fig. 12). EDX data for both crystalline and amorphous components are displayed in Fig. 6.

The amorphous regions of residue are vesiculated (see Fig. 12) and contain Al (see EDX maps in Fig. 13) suggesting a melt origin. The peak pressures and postshock temperatures experienced by particles impacting the Stardust collector Al foils have previously been estimated for several minerals using available Hugoniot and specific heat capacity data: Impacts of olivine, diopside, wollastonite, and pyrrhotite experienced peak pressures of ~ 79 , 87, 69, and 85 GPa and peak post shock temperatures of ~ 1400 , 1600, 1700, and 2600 K, respectively (Wozniakiewicz et al. 2011, 2012a, 2012b). Similar calculations using available hugoniot data for calcite from Kalashnikov et al. (1973)

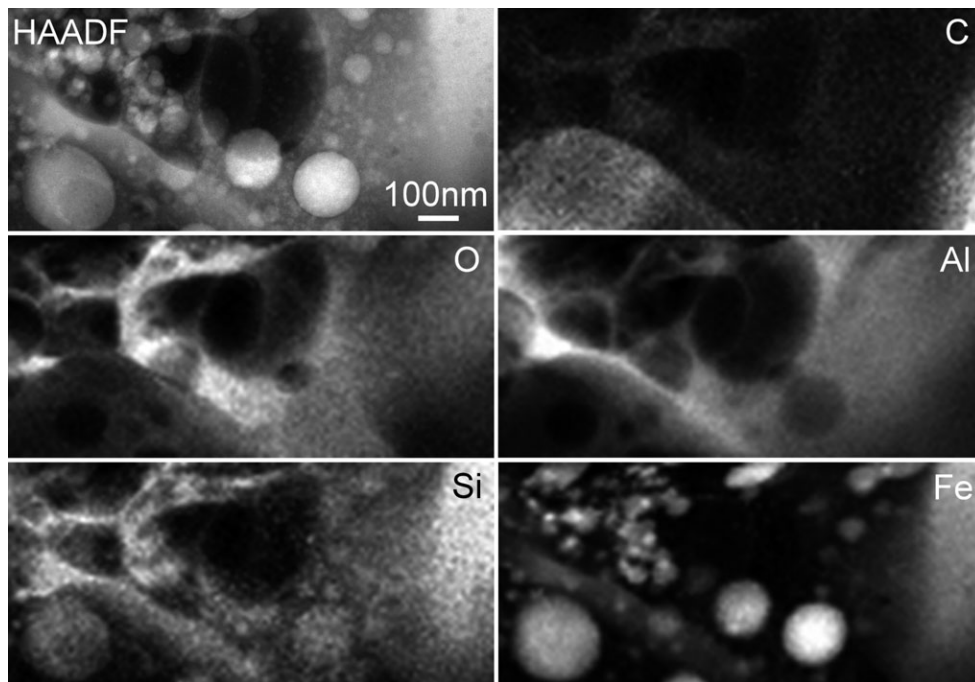


Fig. 11. Elemental abundance maps from $K\alpha$ X-rays of C, O, Al, Si, and Fe taken over a region of the cronstedtite residue section by STEM EDX mapping. Top left panel is the HAADF STEM image of this region.

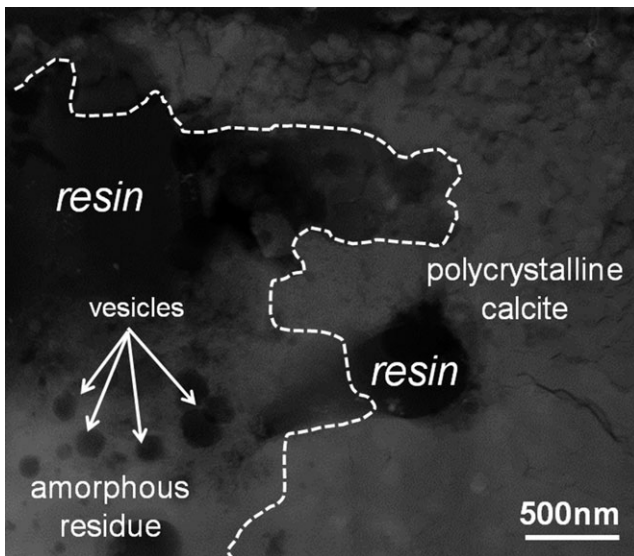


Fig. 12. HAADF STEM image of a region of the calcite residue. The residue is a mixture of polycrystalline (individual crystals <100 nm) and amorphous vesiculated material.

and aluminum 1100 from Marsh (1980), and specific heat capacity data for calcite from Waples and Waples (2004) suggest the peak pressure and postshock temperature experienced by our calcite impactors were 67 GPa and ~ 2700 K, respectively. Such peak values lie above the melt curve of the CaCO_3 phase diagram

(Ivanov and Deutsch 2002), further supporting the idea that these amorphous regions are the result of impact-induced melting of the calcite projectile. As noted previously for lizardite and cronstedtite, the vesiculated regions of residue are likely to have incorporated resin. Although a correction was applied to remove the contribution of the resin to the lizardite and cronstedtite analyses, here it was not possible as the resin shares both of its major elements with calcite (C and O). Instead, care was taken when selecting analysis locations to avoid vesicles and thus minimize resin content, and EDX analyses were performed using a STEM convergent beam (probe) rather than parallel beam, thus maximizing the control over the region from which spectra were obtained. The EDX data collected from these carefully selected regions of amorphous residue are plotted separately on Fig. 6 and exhibit a slight depletion in C and, to varying degrees, in O when compared against the projectile data. The loss of CO_2 from calcite (via decomposition, $\text{CaCO}_3 \rightarrow \text{CaO} + \text{CO}_2$) has been studied previously by several authors investigating the possibility of shock-induced devolatilization in carbonates during planetary impacts and their potential role in modifying planetary atmospheres (e.g., Lange and Ahrens 1983, 1985; Martinez et al. 1995; Ivanov et al. 2002; Langenhorst et al. 2002; Skála et al. 2002). As with the phyllosilicates, however, the amorphous residue does not appear to have undergone complete loss of its

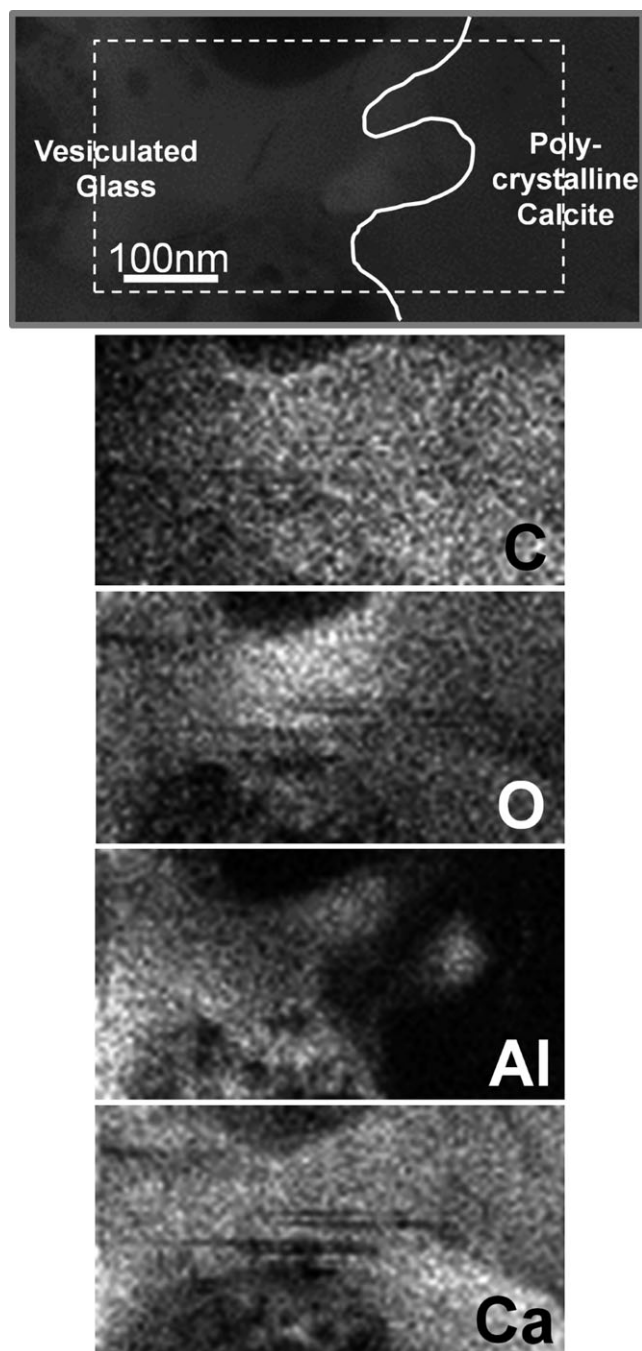


Fig. 13. Elemental abundance maps from $K\alpha$ X-rays of C, O, Al, and Ca taken over a region of the calcite residue section by STEM EDX mapping. Top panel is the HAADF STEM image of this area, with the region being mapped indicated by the dashed box.

volatile components (see cross on Fig. 6 for theoretical decarbonated calcite composition). It also appears to have lost more C than O. These observations suggest that upon impact, as with the phyllosilicates, the Al target has formed an O-scavenging melt that has

incorporated O from impact-released vapor (in this case CO_2).

The crystalline component compositions plot close to those of the preimpact projectile (Fig. 6) and diffraction patterns obtained from these regions are consistent with polycrystalline calcite, suggesting these are surviving, albeit intensely fractured, remnants of the original projectile. This validates the use of the NHM calcite projectile as an elemental standard for the TEM Cliff-Lorimer factors for the low-Z elements. The lack of Al in these crystals (but presence in the melt-derived amorphous residue) indicates that these fragments did not crystallize from the impact melt; however, it remains a possibility that these crystals have undergone solid-state phase changes. Although the peak temperatures and pressures achieved during the impact would result in melting, the range of lower pressures and temperatures experienced elsewhere in the projectile may have resulted in phase transitions. Experiments studying solid phase transitions of calcite have revealed that it undergoes several modifications when subjected to pressure and temperature: Ordinary rhombohedral calcite (calcite I) exists at low temperatures and pressures, but changes to calcite II at low temperatures ($<500\text{ }^\circ\text{C}$) and increasing pressure (up to $\sim 2\text{ GPa}$), calcite III at pressures exceeding 2 GPa and low temperatures ($0\text{ }^\circ\text{C}$ at 2 GPa to $\sim 300\text{ }^\circ\text{C}$ for higher pressures), aragonite at pressures greater than $\sim 2\text{ GPa}$ and intermediate temperatures ($<750\text{ }^\circ\text{C}$ at 2 GPa to $<1400\text{ }^\circ\text{C}$ at 8 GPa), and calcite IV and V at pressures greater than 2 GPa and high temperatures up to the liquidus ($<1500\text{ }^\circ\text{C}$ at 2 GPa to $1750\text{ }^\circ\text{C}$ at 8 GPa). See Suito et al. (2001) and Ivanov and Deutsch (2002) for overviews of calcite phases and discussions of the calcite temperature-pressure phase diagram. Additional experiments have identified a postcalcite III phase transformation at low temperatures and pressures beyond $\sim 15\text{ GPa}$ (Catalli and Williams 2005) and a postaragonite phase transformation occurring at 40 GPa and temperatures above $\sim 1700\text{ }^\circ\text{C}$ (Ono et al. 2005). Our estimates of impact parameters suggest that the pressures and temperatures required for many of these phases might be achieved in various parts of the impactor. However, calcite II, III, IV, and V are unstable at ambient conditions: In their analyses of samples after cooling and decompression, Suito et al. (2001) reported that a mixture of calcite I and aragonite remained in their unmelted samples. Since only calcite was identified during our analyses of the crystalline components in our calcite impact residue, this might suggest that the crystalline calcite portions of the residue represent surviving impactor that has not undergone phase changes. However, Ono et al. (2005) reported that the postaragonite phase is also unstable at

ambient conditions and reverts back to calcite I alone, and Catalli and Williams (2005) reported that their postcalcite III phase had reverted to a phase consistent with a strained calcite I. (They noted that its infrared spectra could also be matched by a calcite I and II mixture, although the instability of calcite II at ambient pressure means this identification is questionable.) It is therefore impossible to say for certain that the calcite crystals in our impact residues have not been subjected to such reversible phase changes during the impact process. The almost instantaneous increase and release of temperature and pressure during an impact are dramatically different to the gradual increase and decrease in temperatures and pressures adopted during the laboratory phase transition experiments, and consequently, we might not expect to observe phase changes at all. However, in our previous investigations of wollastonite impactors, we have observed evidence for the production of new phases after impact, albeit previously unknown from phase transition experiments (Wozniakiewicz et al. 2012b).

Upon impact, calcite has therefore been subjected to fracturing and, in some locations, melting. Those crystalline regions may have been subjected to reversible solid-state phase transitions. In those locations experiencing melting, volatile CO₂ was released and Al incorporated (and oxidized) before solidifying as an amorphous residue.

Implications for Stardust

Our results have shown that, although calcite impactors experience melting during impact into Al foils under Stardust encounter conditions (producing vesiculated, Al-bearing, amorphous residue), portions of the resulting impact residues exhibit the original calcite chemistry and structure. This suggests that if carbonates like calcite were contained within comet Wild 2 grains, some of this material may be preserved, and hence identified, in the Stardust Al foils. We cannot discount the possibility that it may have suffered reversible solid-state phase transformations during collection, but these would not affect mineral identification. In comparison, lizardite and cronstedtite impactors experience extensive melting, loss of volatiles, and incorporation of Al during impacts into Al foils under Stardust encounter conditions. This suggests that if such phyllosilicates were contained within comet Wild 2 grains, they would be unlikely to survive collection by Stardust Al foils intact. The residues of both of these minerals do, however, exhibit several specific and diagnostic characteristics that may allow researchers to interpret precursor phyllosilicate mineralogy: Both exhibit moderate to high vesiculation as a result of their

preimpact volatile content; lizardite residues retain close to preimpact Mg to Si ratios (although several <50 nm native silicon beads were observed within the residue); and cronstedtite residues consist of Fe- and Fe-Si-rich beads (resulting from Fe and Si reduction during impact) embedded in an Fe-bearing, aluminosilicate glass which, when measured in bulk, retains close to original Fe to Si ratios.

We have therefore shown that the ability to interpret precursor mineralogy from TEM analyses of composition and textures observed in Stardust impact crater residues extends to phyllosilicate and carbonate impactors. TEM analyses of 18 Stardust craters performed to date (Leroux et al., 2005; Bridges et al. 2007; Graham et al. 2008, Stroud et al. 2010) have not reported the textures and compositional combinations noted above, providing no clear evidence for these volatile-rich minerals in Wild 2 from the foils. TEM analyses of Stardust foils have, however, focused largely on smaller craters than those analyzed here (<10 μm), because TEM sections can be produced relatively easily by sectioning the whole crater. In contrast, for larger craters, the topography prevents adequate deposition of protective C and Pt layers, and can complicate or limit locations where milling and extraction of sections can be performed. Since most of the mass of material returned by Stardust exists in the larger impacting particles, it is vital that we investigate the residues of the larger craters. Unfortunately, we are unable to perform the preparation procedures adopted here on Stardust samples since embedding whole foils in resin and polishing through craters is simply too wasteful of one-of-a-kind samples. Efforts to investigate residues of larger craters by TEM to date have therefore been limited to a few sections prepared from the crater rims (e.g., Graham et al. 2008); however, preparation methods that seek to raise the floors of these large craters to bring them “within reach” of extraction methods are being explored (e.g., Kearsley et al. 2011) and will hopefully lead to the in-depth analysis of the larger Stardust crater residues by TEM in the near future.

Applying Our TEM Results to Future SEM Analyses: High Resolution Imaging and a New Generation of EDX Detector

TEM is a time-consuming analytical technique, requiring destructive preparation of the crater residue samples by FIB. This preparation method is also selective: a thin section (~100 nm in thickness) is taken from the sample that has a maximum cross sectional area of ~300–400 μm² and more typically 100 μm² (uniformity during the FIB thinning process and

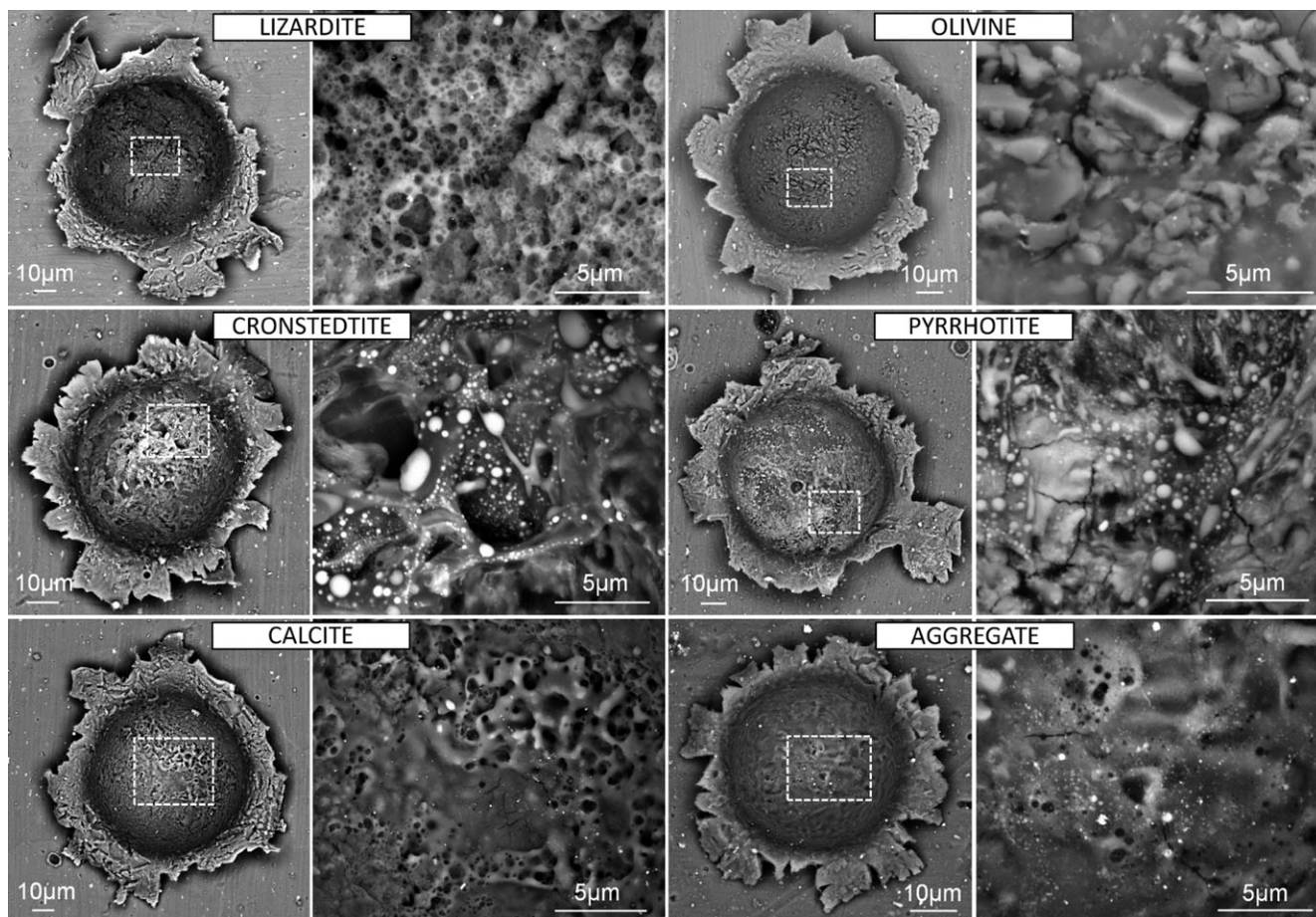


Fig. 14. Low and high magnification BSE SEM images of impact craters and their residues: vesiculated melt residues line craters produced by lizardite, cronstedtite, calcite, pyrrhotite, and aggregate impactors (all containing volatiles), while residues consisting of melt with blocky fragments line craters produced by olivine impactors. The Z-contrast BSE images highlight the presence of bright (high-Z) beads in the cronstedtite, pyrrhotite and aggregate residues as observed in the TEM analyses of such residues reported in this paper, Wozniakiewicz et al. (2011) and Wozniakiewicz et al. (2012a) respectively.

mechanical stability become limiting factors to larger area sections). This means that even if the location of a section is chosen with the greatest of care, there will always be the possibility that the surrounding area (destroyed or damaged during TEM section production) contained different, and potentially important, material. Cometary grains with known origin are unlikely to be returned to Earth for analysis in the near future. The Stardust samples are therefore extremely precious, and researchers go to great efforts to extract the maximum amount of information from each and every grain. For the foils, this means performing whole-crater analyses/measurements using techniques like SEM, prior to selecting areas for further analysis by TEM (once the preparation issues detailed above are resolved). Here, we address whether it is possible to observe the textures and chemistries we have identified by TEM using SEM.

In previous SEM analyses of Stardust analogue craters, Kearsley et al. (2010) described different textures observed in their whole-crater images, noting that organic impactors produce residues with smooth surfaces cut by linear sigmoidal or polygonal fractures, while glass impactors produce smooth residues with little cracking, and crystalline mineral impactors create very rough floors covered by fragmental residue. In Fig. 14 we show similar examples of SEM backscattered electron (BSE) whole-crater images obtained using the FEI Quanta 650 FEG SEM at the NHM. These craters were produced by volatile-bearing impactors lizardite, cronstedtite, calcite, pyrrhotite, and fine-grained aggregates (comprised of olivine, enstatite, and pyrrhotite, held together by polyvinyl acetate adhesive; Kearsley et al. 2013), as well as nonvolatile-bearing olivine impactors. The pyrrhotite, aggregate, and olivine impact craters were produced in separate shots whose

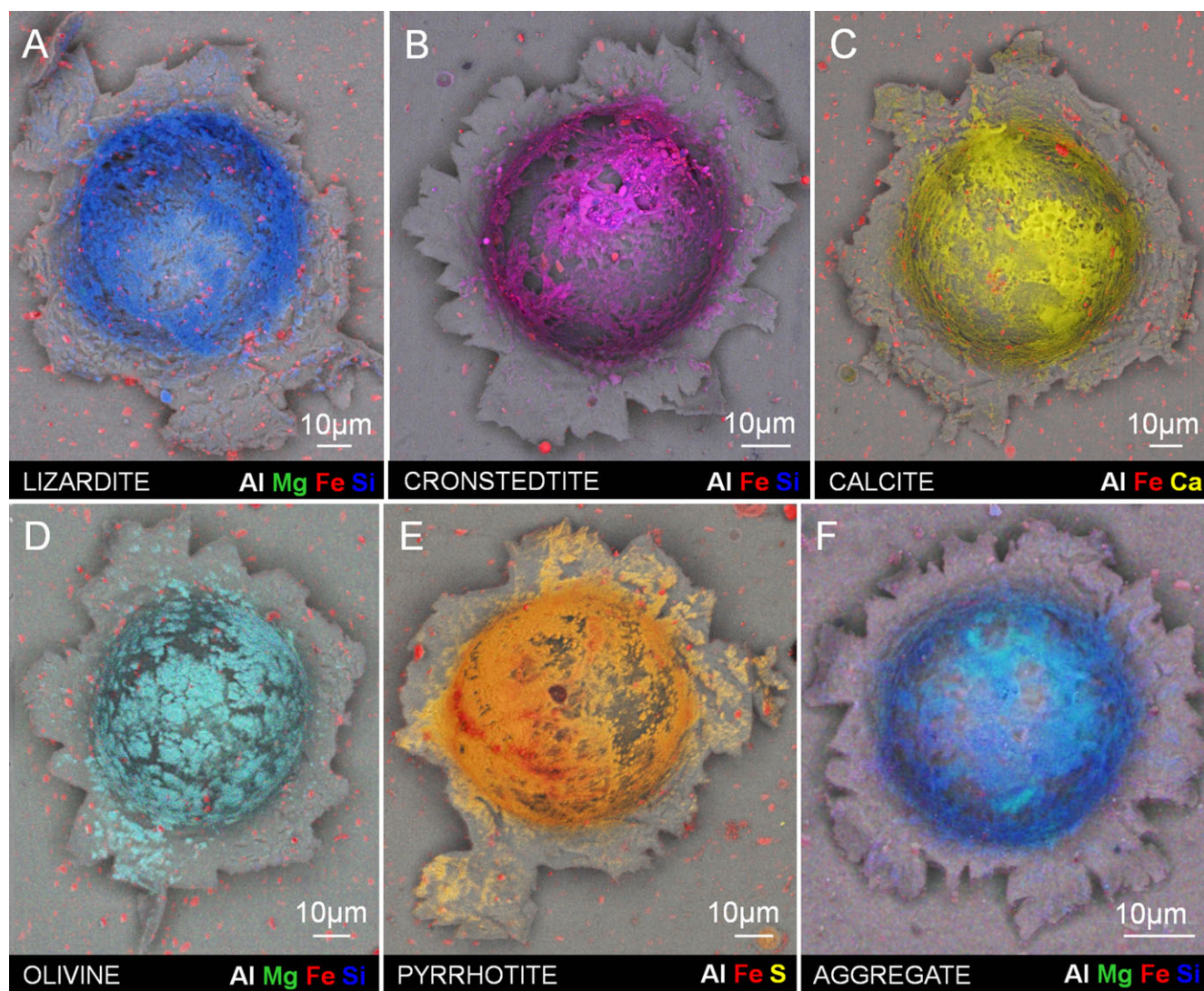


Fig. 15. SEM EDX maps obtained with the Bruker X-flash detector identifying the location of impact residue. These images demonstrate the lack of geometric shadowing and increased coverage of the interiors of Stardust analogue impact craters compared to conventional, inclined detectors. Maps were obtained at 15 kV, with a spatial resolution of ~ 500 nm per pixel.

details (shot number and velocity) can be found in table 1 of Wozniakiewicz et al. (2012a). Accompanying these are high magnification BSE images of areas within these craters showing details of residue textures. These images clearly show the characteristic vesiculated textures observed by TEM for the impact melt residues of lizardite, cronstedtite, and calcite detailed in this paper, and for the pyrrhotite and aggregate impactors detailed previously (Wozniakiewicz et al. 2011, 2012a). In comparison, the olivine residue consists of melt with blocky fragments consistent with TEM analyses detailed in Wozniakiewicz et al. (2012a) and observed previously by Kearsley et al. (2010). These melt residue textures, which are a clear indication of whether the precursor grain contained volatiles, are therefore clearly visible in

SEM images. The Z-contrast exhibited in the BSE SEM images of Fig. 14 also appear to highlight details of the Fe- and/or Fe-Si-rich beads in the impact melts of cronstedtite, pyrrhotite, and aggregate residues as observed by TEM analyses: Bright (high-Z) beads are visible among the residue of these craters.

To further interpret the original mineralogy of these residues by SEM, chemical data are required to complement these textural observations. SEM EDX analyses of impact residues have been complicated in the past by the rough topography of craters; conventional EDX detectors are mounted to one side of the pole piece (typically at an inclination of $\sim 40^\circ$), resulting in shadowing of the majority of the crater floor (see fig. 2 in Wozniakiewicz et al. 2009).

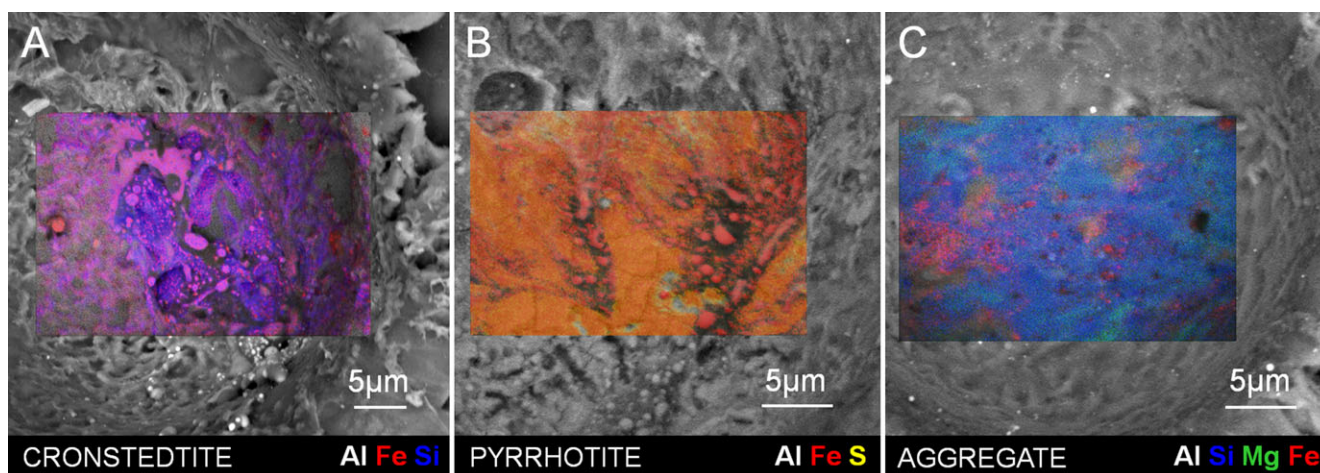


Fig. 16. SEM EDX maps obtained with the Bruker XFlash detector over small areas within the cronstedtite, pyrrhotite, and aggregate craters: TEM analyses (reported here and in Wozniakiewicz et al. 2011, 2012a) show that impacts of these three minerals produce multicomponent residues. This detector enables the collection of maps that show these different phases at submicrometer spatial resolution. Maps were obtained at 5 or 6 kV, with a spatial resolution of ~ 50 nm per pixel.

Consequently, details of chemistry could only be obtained from those regions of residue in-sight of the detector—typically a narrow band around the crater lip and on the steep crater wall. However, a new generation of EDX detectors is now available that could revolutionize the analysis of Stardust craters: the Bruker XFlash FlatQUAD SDD is an annular, multisegment EDX detector that is inserted beneath the pole piece, giving very high count rates from a high take-off angle and from a wide range of azimuth angles. This detector, which has recently been installed on the FEI Quanta 650 FEG SEM at the NHM, can map impact residues at high resolution over the entire crater floor (Kearsley et al. 2011, 2013). Figure 15 shows the EDX maps obtained by this detector for the craters in Fig. 14. Mapping was performed at an accelerating voltage of 15 kV, collecting for 1 h. Maps were contrast stretched, then colored and combined to show the distribution of elements. Additional maps were obtained at 5 or 6 kV to obtain higher spatial resolution over smaller areas within the cronstedtite, pyrrhotite, and aggregate craters to investigate the multicomponent nature of these residues. These are overlain on the corresponding BSE images in Fig. 16 and clearly exhibit variations in chemistry that correlate with the Z-contrast and textural variations observed in the BSE images. Although quantitative major element abundances cannot be obtained by SEM for such complicated samples (with rough topography and multicomponent nature) the maps obtained with the new generation annular SDD EDX detector provide the necessary data to make a reasonable assessment of the original mineralogy when combined with Z-contrast and textural data provided by SEM imaging. In order to obtain quantitative chemical

data, assess the incorporation of Al into melt and study the crystallinity (or amorphous nature) of the residue components, TEM is required, and these whole-crater SEM EDX maps combined with high magnification imaging would also be invaluable to the selection of appropriate areas for TEM section preparation, as well as other microanalysis techniques (e.g., secondary ion mass spectrometry; Snead et al. 2015).

CONCLUSIONS

We have simulated the Stardust encounter conditions using the two-stage light-gas gun to determine whether phyllosilicates and carbonates remain recognizable after capture by the Al foils of the spacecraft's collector. Our TEM analyses of, and direct comparison between, the pre- and postimpacted samples of these minerals have shown that

1. The phyllosilicates, lizardite and cronstedtite, appear completely melted by impact, resulting in loss of their characteristic layered structures and release of volatiles, producing moderately to highly vesiculated amorphous residues.
2. Despite the loss of volatiles from phyllosilicates, bulk chemical data indicates retention of near-original cation to Si ratios (Mg to Si for lizardite and Fe to Si for cronstedtite).
3. Closer inspection of lizardite and cronstedtite residues reveals native silicon, Fe-rich and Fe-Si-rich beads on a submicron scale. The production of these phases requires reducing conditions that we believe are produced by the presence of O-scavenging molten Al from the target foils. Their identification indicates rapid diffusion and, in at

least the case of cronstedtite where these segregated beads were large enough to ascertain crystallinity, crystallization of new phases even in the short timescales applicable to such impacts.

4. The carbonate mineral calcite also experiences alteration, although to a lesser degree than the phyllosilicates: some regions of the projectile experience melting upon impact, resulting in the loss of volatiles (CO₂) and production of vesiculated amorphous residues; however, a large portion of the residue retains the original calcite mineralogy.
5. Those regions of phyllosilicate and carbonate projectiles that experience melting upon impact incorporate Al from the target foils.
6. Although those regions of the projectiles that undergo melting experience some degree of dehydration (phyllosilicates) or decarbonation (carbonates), they appear to retain some fraction of the O that is released. This is likely the result of the incorporation and oxidation of molten Al from the foil target.
7. It may be possible to interpret a phyllosilicate precursor in Stardust impact craters based on the presence of vesiculated amorphous residues and appropriate bulk major element ratios.
8. It may be possible to identify carbonates in Stardust impact craters by the presence of surviving/remaining mineralogy.

The Stardust Al foils therefore represent a valuable sample set for the investigation of cometary phyllosilicates and carbonates. To date, TEM analyses of Stardust craters have found evidence of neither phyllosilicates nor carbonates. This nonobservation based on the limited number of craters analyzed by TEM (18 craters to date) suggests that fewer than 6% had significant phyllosilicate or carbonate content. However, we note that TEM analyses of residues within the largest craters (not merely on their FIB-accessible rims) are still to be performed. These TEM analyses require the development of preparation techniques that provide permissible access to the residue within these large craters. In the meantime, SEM imaging and EDX mapping may facilitate interpretations of impactor mineralogy from crater residues: We have shown that the characteristic vesiculated textures associated with impact melts produced by volatile-bearing impactors are clearly visible in SEM images and that, combined with compositional data from a new generation of SEM EDX detector, it is possible to make interpretations as to the precursor impactor mineralogy rapidly and nondestructively.

Acknowledgments—We thank Z. Gainsforth and the AE D. Brownlee for their helpful comments and suggestions

during the review of this manuscript. We thank NASA for providing Al foils, STFC for support of the LGG. Parts of this work were performed under the auspices of the U.S. DOE by LLNL under Contract DE-AC52-07NA27344. This work was supported by grants NASA NNH07AG46I and NNX14AH86G to HAI & LDRD 09-ERI-004 to JPB.

Editorial Handling—Dr. Donald Brownlee

REFERENCES

- Anand M., Taylor L. A., Nazarov M. A., Shu J., Mao H.-K., and Hemley J. 2004. Space weathering on airless planetary bodies: Clues from the lunar mineral hapkeite. *Proceedings of the National Academy of Sciences* 101:6847–6851.
- Badjukov D. D. and Petrova T. L. 1991. Shock induced interaction between metal iron and silicates. *Proceedings, 22nd Lunar and Planetary Science Conference*. p. 41.
- Batson P. E. 1991. Current trends for EELS studies in physics. *Microscopy, Microanalysis, Microstructures* 2:395–402.
- Berger E. L., Zega T. J., Keller L. P., and Lauretta D. S. 2011. Evidence for aqueous activity on comet 81P/Wild 2 from sulfide mineral assemblages in Stardust samples and CI chondrites. *Geochimica et Cosmochimica Acta* 75:3501–3513.
- Bradley J. P. 2003. Interplanetary dust particles. In *Meteorites, comets and planets*, edited by Davis A. M. Treatise on Geochemistry, vol. 1, executive editors Holland H. D. and Turekian K. K. Oxford: Elsevier-Pergamon. pp. 689–711.
- Bradley J. P. 2013. Early solar nebula grains—Interplanetary dust particles. In *Meteorites and cosmochemical processes*, 2nd ed., edited by Davis A. M. Treatise on Geochemistry, vol. 1. Oxford: Elsevier-Pergamon. pp. 287–308.
- Bradley J. P., Keller L. P., Snow T. P., Hanner M. S., Flynn G. J., Gezo J. C., Clemett S. J., Brownlee D. E., and Bowey J. E. 1999. An infrared spectral match between GEMS and interstellar grains. *Science* 285:1716–1718.
- Bridges J. C., Franchi I. A., and Green S. F. 2007. Stardust microcrater residue compositional groups (abstract #2180). 38th Lunar and Planetary Science Conference. CD-ROM.
- Brownlee D. E. 2003. Comets. In *Meteorites, comets and planets*, edited by Davis A. M. Treatise on Geochemistry, vol. 1, executive editors Holland H. D. and Turekian K. K. Oxford: Elsevier-Pergamon. pp. 663–688.
- Brownlee D. E., Joswiak D. J., Love S. G., Nier A. O., Schlutter D. J., and Bradley J. P. 1993. Properties of cometary and asteroidal IDPs identified by He temperature-release profiles. *Meteoritics* 28:332.
- Brownlee D. E., Joswiak D. J., and Love S. G. 1994. Identification and analysis of cometary IDPs. *Proceedings, 25th Lunar and Planetary Science Conference*. p. 185.
- Brownlee D., Joswiak D. J., Schlutter D. J., Pepin R. O., Bradley J. P., and Love S. G. 1995. Identification of individual cometary IDPs by thermally stepped He release. 25th Lunar and Planetary Science Conference. p. 183.
- Brownlee D. E., Tsou P., Anderson J. D., Hanner M. S., Newburn R. L., Sekanina Z., Clark B. C., Hörz F., Zolensky M. E., Kissel J., McDonnell J. A. M., Sandford S. A., and Tuzzolino A. J. 2003. Stardust: Comet and interstellar dust sample return mission. *Journal of Geophysical Research (Planets)* 108(E10):8111.

- Brownlee D. E., Tsou P., Aléon J., Alexander C. M. O'D., Araki T., Bajt S., Baratta G. A., Bastien R., Bland P., Bleuet P., Borg J., Bradley J. P., Brearley A., Brenker F., Brennan S., Bridges J. C., Browning N., Brucato J. R., Brucato H., Bullock E., Burchell M. J., Busemann H., Butterworth A., Chaussidon M., Chevront A., Chi M., Cintala M. J., Clark B. C., Clemett S. J., Cody G., Colangeli L., Cooper G., Cordier P. G., Daghlian C., Dai Z., D'Hendecourt L., Djouadi Z., Dominguez G., Duxbury T., Dworkin J. P., Ebel D., Economou T. E., Fairey S. A. J., Fallon S., Ferrini G., Ferroir T., Fleckenstein H., Floss C., Flynn G., Franchi I. A., Fries M., Gainsforth Z., Gallien J.-P., Genge M., Gilles M. K., Gillet P., Gilmour J., Glavin D. P., Gounelle M., Grady M. M., Graham G. A., Grant P. G., Green S. F., Grossemy F., Grossman L., Grossman J., Guan Y., Hagiya K., Harvey R., Heck P., Herzog G. F., Hoppe P., Hörz F., Huth J., Hutcheon I. D., Ishii H., Ito M., Jacob D., Jacobsen C., Jacobsen S., Joswiak D., Kearsley A. T., Keller L., Khodja H., Kilcoyne A. L. D., Kissel J., Krot A., Langenhorst F., Lanzirotti A., Le L., Leshin L., Leitner J., Lemelle L., Leroux H., Liu M.-C., Luening K., Lyon I., MacPherson G., Marcus M. A., Marhas K., Matrajt G., Meibom A., Mennella V., Messenger K., Mikouchi T., Mostefaoui S., Nakamura T., Nakano T., Newville M., Nittler L. R., Ohnishi I., Ohsumi K., Okudaira K., Papanastassiou D. A., Palma R., Palumbo M. O., Pepin R. E., Perkins D., Perronnet M., Pianetta P., Rao W., Rietmeijer F., Robert F., Rost D., Rotundi A., Ryan R., Sandford S. A., Schwandt C. S., See T. H., Schlutter D., Sheffield-Parker J. A., Simionovici S., Sittinsky S. I., Snead C. J., Spencer M. K., Stadermann F. J., Steele A., Stephan T., Stroud R., Susini J., Sutton S. R., Taheri M., Taylor S., Teslich N., Tomeoka K., Tomioka N., Toppani A., Trigo-Rodríguez J. M., Troadec D., Tsuchiyama A., Tuzzolino A. J., Tyliczszak T., Uesugi K., Velbel M., Vellenga J., Vicenzi E., Vincze L., Warren J., Weber I., Weisberg M., Westphal A. J., Wirick S., Wooden D., Wopenka B., Wozniakiewicz P. A., Wright I., Yabuta H., Yano H., Young E. D., Zare R. N., Zega T., Ziegler K., Zimmerman L., Zinner E., and Zolensky M. 2006. Comet 81P/Wild 2 under a microscope. *Science* 314:1711–1716.
- Burchell M. J. and Kearsley A. T. 2009. Short period Jupiter family comets after Stardust. *Planetary and Space Science* 57:1146–1161.
- Burchell M. J., Cole M. J., McDonnell J. A. M., and Zarnecki J. C. 1999. Hypervelocity impact studies using the 2 MV Van de Graaff dust accelerator and two stage light gas gun of the University of Kent at Canterbury. *Measurement Science and Technology* 10:41–50.
- Burchell M. J., Graham G. A., and Kearsley A. T. 2006. Cosmic dust collection in aerogel. *Annual Reviews of Earth and Planetary Sciences* 34:385–418.
- Burchell M. J., Foster N. J., Kearsley A. T., and Creighton J. A. 2008a. Identification of mineral impactors in hypervelocity impact craters in aluminum by Raman spectroscopy of residues. *Meteoritics & Planetary Science* 43:135–142.
- Burchell M. J., Fairey S. A. J., Wozniakiewicz P. J., Brownlee D. E., Hörz F., Kearsley A. T., See T. H., Tsou P., Westphal A., Green S. F., Trigo-Rodríguez J. M., and Dominguez G. 2008b. Characteristics of cometary dust tracks in Stardust aerogel and laboratory calibrations. *Meteoritics & Planetary Science* 43:23–40.
- Catali K., and Williams Q. 2005. A high-pressure phase transformation of calcite-III. *American Mineralogist* 90:1679–1682.
- Ciesla F. J., Lauretta D. S., Chen B. A., and Hood L. L. 2003. A nebula origin for chondritic fine-grained phyllosilicates. *Science* 299:549–552.
- Croat T. K., Floss C., Haas B. A., Burchell M. J., and Kearsley A. T. 2015. Survival of refractory presolar grain analogs during Stardust-like impact into Al foils: Implications for Wild 2 presolar grain abundances and study of the cometary fine-fraction. *Meteoritics & Planetary Science* 50:1378–1391.
- Crovisier J., Leech K., Bockelee-Morvan D., Brooke T. Y., Hanner M. S., Altieri B., Keller H. U., and Lellouch E. 1997. The spectrum of Hale-Bopp observed with ISO 2.9 AU from the Sun. *Science* 275:1904–1907.
- Deer W. A., Howie R. A., and Zussman J. 1992. *An introduction to the rock forming minerals*, 2nd ed. Harlow, UK: Pearson Education Limited. 696 p.
- Essene E. J. and Fisher D. C. 1986. Lightning strike fusion: Extreme reduction and metal-silicate liquid immiscibility. *Science* 234:189–193.
- Fiske P. S., Nellis W. J., Lipp M., Lorenzana H., Kikuchi M., and Syono Y. 1995. Pseudotachylites generated in shock experiments: Implications for impact cratering products and processes. *Science* 270:281–283.
- Floss C., Stadermann F. J., Kearsley A. T., Burchell M. J., and Ong W. J. 2014. The abundance of presolar grains in Comet 81P/Wild 2. *The Astrophysical Journal* 763:140.
- Flynn G. J., Leroux H., Tomeoka K., Tomioka N., Ohnishi I., Mikouchi T., Wirick S., Keller L. P., Jacobsen C., and Sandford S. A. 2008. Carbonate in comets: A comparison of comets 1P/Halley, 9P/Tempel 1 and 81P/Wild 2 (abstract #1979). 39th Lunar and Planetary Science Conference. CD-ROM.
- Fomenkova M. N., Kerridge J. F., Marti K., and McFadden L.-A. 1992. Compositional trends in rock-forming elements of comet Halley dust. *Science* 258:266–269.
- Gerasimov M. V., Yakovlev O. I., Dikov Y. P., and Wlotzka F. 2000. Evaporative differentiation of impact-produced melts: Laser-simulation experiments and comparison with impact glasses from the Logoiski crater. In *Large meteorite impacts III*, edited by Kenkmann T., Hörz F., and Deutsch A. *Geological Society of America, Special Paper* 384:351–366.
- Graham G. A., Teslich N. E., Kearsley A. T., Stadermann F. J., Stroud R. M., Dai Z., Ishii H. A., Hutcheon I. D., Bajt S., Snead C. J., Weber P. K., and Bradley J. P. 2008. Applied focused ion beam techniques for sample preparation of astromaterials for integrated nanoanalysis. *Meteoritics & Planetary Science* 43:561–569.
- Hanner M. S., Lynch D. K., and Russell R. W. 1994. The 8–13 micron spectra of comets and the composition of silicate grains. *The Astrophysical Journal* 425:274–285.
- Hashimoto A. 1983. Evaporative metamorphism in the early solar nebula—Evaporation experiments on the melt FeO-MgO-SiO₂-CaO-Al₂O₃ and chemical fractionations of primitive materials. *Geochemical Journal* 17:111–145.
- Henning T. and Mutschke H. 1997. Low-temperature infrared properties of cosmic dust analogues. *Astronomy & Astrophysics* 327:743–754.

- Herrin J. S., Mittlefehldt D. M., and Jones J. H. 2008. Petrogenesis of Fe,Si-metals in brecciated ureilites (abstract #5327). 71st Meeting of the Meteoritical Society.
- Hörz F., Bastien R., Borg J., Bradley J. P., Bridges J. C., Brownlee D. E., Burchell M. J., Cintala M. J., Dai Z. R., Djouadi Z., Dominguez G., Economou T. E., Fairley S. A. J., Floss C., Franchi I. A., Graham G. A., Green S. F., Heck H., Hoppe P., Huth J., Ishii H., Kearsley A. T., Kissel J., Leitner J., Leroux H., Marhas M., Messenger K., Schwandt C. S., See T. H., Snead S., Stadermann F. J., Stephan T., Stroud R., Teslich N., Trigo-Rodríguez J. M., Tuzzolino A. J., Troadec D., Tsou P., Warren J., Westphal A., Wozniakiewicz P. J., Wright I., and Zinner E. 2006. Impact features on Stardust and comet Wild 2 dust. *Science* 314:1716–1719.
- Ishii H. A., Bradley J. P., Dai Z. R., Chi M., Kearsley A. T., Burchell M. J., Browning N. D., and Molster F. 2008. Comparison of comet 81P/Wild 2 dust with interplanetary dust from comets. *Science* 319:447–450.
- Ivanov B. and Deutsch A. 2002. The phase diagram of CaCO₃ in relation to shock compression and decomposition. *Physics of Planetary Interiors* 129:131–143.
- Ivanov B. A., Langenhorst F., Deutsch A., and Hornemann U. 2002. How strong was the impact-induced CO₂ degassing in the K/T event? Numerical modelling of laboratory experiments. In *Catastrophic events and mass extinctions: Impact and beyond*, edited by Koeberl C. and MacLeod K. G. *Geological Society of America, Special Paper* 356:587–594.
- Joswiak D. J., Brownlee D. E., Matrajt G., Westphal A. J., Snead C. J., and Gainsforth Z. 2012. Comprehensive examination of large mineral and rock fragments in Stardust tracks: Mineralogy, analogous extraterrestrial materials, and source regions. *Meteoritics & Planetary Science* 47:471–524.
- Kalashnikov N. G., Pavlovskii M. N., Simakov G. V., and Trunin R. F. 1973. Dynamic compressibility of the minerals of calcite group. *Izvestiya Akademii Nauk SSSR Fizika Zemli* 2:23–29.
- Kearsley A. T., Burchell M. J., Hörz F., Cole M. J., and Schwandt C. S. 2006. Laboratory simulation of impacts on aluminium foils of the Stardust spacecraft: Calibration of dust particle size from comet Wild-2. *Meteoritics & Planetary Science* 41:167–180.
- Kearsley A. T., Graham G. A., Burchell M. J., Cole M. J., Dai Z. R., Teslich N., Bradley J. P., Chater R., Wozniakiewicz P. J., Spratt J., and Jones G. 2007. Analytical scanning and transmission electron microscopy of laboratory impacts on Stardust aluminium foils: Interpreting impact crater morphology and the composition of impact residues. *Meteoritics & Planetary Science* 42:191–210.
- Kearsley A. T., Borg J., Graham G. A., Burchell M. J., Cole M. J., Leroux H., Bridges J. C., Hörz F., Wozniakiewicz P. J., Bland P. A., Bradley J. P., Dai Z. R., Teslich N., See T., Hoppe P., Heck P. R., Huth J., Stadermann F. J., Floss C., Marhas K., Stephan T., and Leitner J. 2008. Dust from comet Wild 2: Interpreting particle size, shape, structure and composition from impact features on the Stardust aluminium foils. *Meteoritics & Planetary Science* 43:41–74.
- Kearsley A. T., Burchell M. J., Price M. C., Graham G. A., Wozniakiewicz P. J., Cole M. J., Foster N. J., and Teslich N. 2009. Interpretation of Wild 2 dust fine structure: Comparison of Stardust aluminium foil craters to the three-dimensional shape of experimental impacts by artificial aggregate particles and meteorite powders. *Meteoritics & Planetary Science* 44:1489–1509.
- Kearsley A. T., Burchell M. J., Price M. C., Green S. F., Franchi I. A., Bridges J. C., Starkey N., and Cole M. C. 2010. Distinctive impact craters are formed by organic-rich cometary dust grains (abstract #1435). 41st Lunar and Planetary Science Conference. CD-ROM.
- Kearsley A. T., Burchell M. J., Price M. C., Cole M. J., Wozniakiewicz P. J., Ishii H. A., Teslich N., Bradley J. P., and Salge T. 2011. Cometary dust residue in large Stardust foil craters: How much survives, and how to safely extract it for analysis (abstract #5380). 74th Meeting of the Meteoritical Society. *Meteoritics & Planetary Science* 46.
- Kearsley A. T., Salge T., Wozniakiewicz P. J., Price M. C., Terborg R., Burchell M. J., and Cole M. J. 2013. Preservation and modification of fine-grained cometary dust captured by Stardust: The fate of aggregate components in hypervelocity impacts on aluminium foil (abstract #1910). 44th Lunar and Planetary Science Conference. CD-ROM.
- Keil K., Berkley J. L., and Fuchs L. H. 1982. Suessite, Fe₃Si: A new mineral in the North Haig ureilite. *American Mineralogist* 67:126–131.
- Lange M. A. and Ahrens T. J. 1983. Shock-induced CO₂-production from carbonates and a proto-CO₂-atmosphere on the Earth. *Proceedings, 14th Lunar and Planetary Science Conference*. p. 419.
- Lange M. A. and Ahrens T. J. 1985. Shock-induced CO₂ loss from CaCO₃; implications for early planetary atmospheres. *Earth and Planetary Science Letters* 77:409–418.
- Langenhorst F. 2002. Shock metamorphism of some minerals: Basic introduction and microstructural observations. *Bulletin of the Czech Geological Survey* 77:265–282.
- Langenhorst F., Boustie M., Deutsch A., Hornemann U., Matignon C., Migault A., and Romain J. P. 2002. Experimental techniques for the simulation of shock metamorphism: A case study on calcite. In *High-pressure shock compression of solids V—Shock chemistry with applications to meteorite impacts*, edited by Davison L., Horie Y., and Sekine T. New York: Springer. pp. 1–27.
- Leroux H., Stroud R. M., Dai Z.-R., Graham G. A., Troadec D., Bradley J. P., Teslich N., Borg J., Kearsley A. T., and Hörz F. 2005. Transmission electron microscopy of cometary residues from micron-sized craters in the Stardust Al foils. *Meteoritics & Planetary Science* 43:143–160.
- Lisse C. M., VanCleve J., Adams A. C., A'Hearn M. F., Fernandez Y. R., Farnham T. L., Armus L., Grillmair C. J., Ingalls J., Belton M. J. S., Groussin O., McFadden L. A., Meech K. J., Schultz P. H., Clark B. C., Feaga L. M., and Sunshine J. M. 2006. Spitzer spectral observations of the Deep Impact ejecta. *Science* 313:635–640.
- Maas R. W., Ney E. P., and Woolf N. J. 1970. The 10-micron emission of comet Bennett 1969i. *The Astrophysical Journal* 160:L101–L104.
- Marsh S. P. 1980. *LASL shock hugoniot data*. Los Angeles: University of California Press. p. 674.
- Martinez I., Deutsch A., Schärer U., Ildefonse P., Guyot F., and Agrinier P. 1995. Shock recovery experiments on dolomite and thermodynamical modeling of impact-induced decarbonation. *Journal of Geophysical Research* 100(B8):15,465–15,476.

- Melosh H. J. 1989. *Impact cratering—A geologic process*. New York: Oxford University Press. 245 p.
- Min M., Waters L. B. F. M., de Koter A., Hovenier J. W., Keller L. P., and Markwick-Kemper F. 2008. The shape and composition of interstellar silicate grains. *Astronomy & Astrophysics* 462:667–676.
- Molster F. J. and Waters L. B. F. M. 2003. Mineralogy of interstellar and circumstellar dust. In *Astromineralogy*, edited by Henning T. Heidelberg: Springer. pp. 121–170.
- Nazarov M. A., Demidova S. I., Anosova M. O., Kostitsyn Y. A., Ntaflos T., and Brandstaetter F. 2012. Native silicon and iron silicides in the Dhofar 280 lunar meteorite. *Petrology* 20:506–519.
- Nazarov M. A., Shornikov S. I., and Demidova S. I. 2015. Origin of native silicon in iron silicides in the Dhofar 280 lunar meteorite. *Petrology* 23:168–175.
- Noguchi T., Nakamura T., Okudaira K., Yano H., Sugita S., and Burchell M. J. 2007. Thermal alteration of hydrated minerals during hypervelocity capture to silica aerogel at the flyby speed of Stardust. *Meteoritics & Planetary Science* 42:357–372.
- Ono S., Kikegawa T., Ohisho Y., and Tsuchiya J. 2005. Post-aragonite phase transformation in CaCO₃ at 40 GPa. *American Mineralogist* 90:667–671.
- Price M. C., Kearsley A. T., Burchell M. J., Hörz F., Borg J., Bridges J. C., Cole M. J., Floss C., Graham G., Green S. F., Hoppe P., Leroux H., Marhas K. K., Park N., Stroud R., Stadermann F. J., Teslich N., and Wozniakiewicz P. J. 2010. Comet 81P / Wild 2: The size distribution of finer (sub 10-micrometre) dust collected by the Stardust spacecraft. *Meteoritics & Planetary Science* 45:1409–1428.
- Rietmeijer F. J. M., Nakamura T., Tsuchiyama A., Uesugi K., Nakano T., and Leroux H. 2008. Origin and formation of iron silicide phases in the aerogel of the Stardust mission. *Meteoritics & Planetary Science* 43:121–134.
- Ross A. J., Downes H., Smith C. L., and Jones A. P. 2009. Highly reduced metals and sulphides in ureilites: Remnants of the UPB core? (abstract #5269). 72nd Meeting of the Meteoritical Society. *Meteoritics & Planetary Science* 44.
- Rowan L. R. and Ahrens T. J. 1994. Observations of impact-induced molten metal-silicate partitioning. *Earth and Planetary Science Letters* 122:77–88.
- Sandford S. A. and Walker R. M. 1985. Laboratory infrared transmission spectra of individual interplanetary dust particles from 2.5 to 25 microns. *The Astrophysical Journal* 291:838–851.
- Schneider R., Woltersdorf J., and Lichtenberger O. 1996. ELNES across interlayers in SiC(Nicalon) fibre-reinforced Duran glass. *Journal of Physics D: Applied Physics* 29:1709–1715.
- Skála R., Ederová J., Matejka P., and Hörz F. 2002. Mineralogical investigations of experimentally shocked dolomite: Implications for the outgassing of carbonates. In *Catastrophic events and mass extinctions: Impact and beyond*, edited by Koeberl C. and MacLeod K. G. *Geological Society of America, Special Paper* 356:571–586.
- Smith C. L., Ross A. J., and Downes H. 2010. Iron silicide in polymict ureilites—Recording the complex history of the ureilite parent body (abstract #5221). 73rd Meeting of the Meteoritical Society. *Meteoritics & Planetary Science* 45.
- Snead C. J., McKeegan K. D., Boehnke P., and Kearsley A. T. 2015. Further oxygen isotope measurements for two cometary impact crater residues: Still like chondrites (abstract #2621). 46th Lunar and Planetary Science Conference. CD-ROM.
- Spicuzza M. J., Valley J. W., Fournelle J., Huberty J. M., and Treiman A. 2011. Native silicon and Fe-silicides from the Apollo 16 lunar regolith: Extreme reduction, metal-silicate immiscibility, and shock melting (abstract #2231). 42nd Lunar and Planetary Science Conference. CD-ROM.
- Stroud R. M., Koch I. M., Bassim N. D., Piccard Y. N., and Nittler L. R. 2010. Structure and composition of comet Wild 2 residues in sub-micron to micro-sized craters (abstract #1792). 41st Lunar and Planetary Science Conference. CD-ROM.
- Suito K., Namba J., Horikawa T., Taniguchi Y., Sakurai N., Kobayashi M., Onodera A., Shimomura O., and Kikegawa T. 2001. Phase relations of CaCO₃ at high pressure and high temperature. *American Mineralogist* 86:997–1002.
- Toppani A., Robert F., Libourel G., de Donato P., Barres O., d’Hendecourt L., and Ghanbaja J. 2005. A “dry” condensation origin for circumstellar carbonates. *Nature* 437:1121–1124.
- Trigo-Rodríguez J. M., Dominguez G., Burchell M. J., Hörz F., and Llorca J. 2008. Bulbous tracks arising from hypervelocity capture in aerogel. *Meteoritics & Planetary Science* 43:75–86.
- Verniani F. 1969. Structure and fragmentation of meteoroids. *Space Science Reviews* 10:230–261.
- Waples D. W., and Waples J. S. 2004. A review and evaluation of specific heat capacities of rocks, minerals, and subsurface fluids. Part 1: Minerals and nonporous rocks. *Natural Resources Research* 13:97–122.
- Wirick S., Leroux H., Tomeoka K., Zolensky M., Tyliszczak T., Butterworth A., Tomioka N., Ohnishi I., Nakamura Messenger K., Sandford S., Keller L., and Jacobsen C. 2007. Carbonates found in Stardust aerogel tracks (abstract 1534). 38th Lunar and Planetary Science Conference. CD-ROM.
- Wozniakiewicz P. J., Kearsley A. T., Burchell M. J., Foster N. J., Cole M. J., Bland P. A., and Russell S. A. R. 2009. Analysis of residues resulting from laboratory impacts into aluminum 1100 foil: Implications for Stardust crater analyses. *Meteoritics & Planetary Science* 44:1541–1559.
- Wozniakiewicz P. J., Ishii H. A., Kearsley A. T., Burchell M. J., Bland P. A., Bradley J. P., Dai Z. R., Teslich N., Collins G. S., Cole M. J., and Russell S. S. 2011. Investigation of iron sulfide impact crater residues: A combined analysis by scanning and transmission electron microscopy. *Meteoritics & Planetary Science* 46:1007–1024.
- Wozniakiewicz P. J., Ishii H. A., Kearsley A. T., Burchell M. J., Bradley J. P., Price M. C., Teslich N., Lee M., and Cole M. J. 2012a. Stardust impact analogues: Resolving pre- and post-impact mineralogy in Stardust Al foils. *Meteoritics & Planetary Science* 47:708–728.
- Wozniakiewicz P. J., Kearsley A. T., Ishii H. A., Burchell M. J., Bradley J. P., Teslich N., Cole M. C., and Price M. C. 2012b. The origin of crystalline residues in Stardust Al foils: Surviving cometary dust or crystallized impact melts? *Meteoritics & Planetary Science* 47:660–670.
- Zolensky M. E., Pieters C., Clark B., and Papike J. J. 2000. Small is beautiful: The analysis of nanogram-sized astromaterials. *Meteoritics & Planetary Science* 35:9–29.

- Zolensky M. E., Zega T. J., Yano H., Wirick S., Westphal A. J., Weisberg M. K., Weber I., Warren J. L., Velbel M. A., Tsuchiyama A., Tsou P., Toppani A., Tomioka N., Tomeoka K., Teslich N., Taheri M., Susini J., Stroud R., Stephan T., Stadermann F. J., Snead C. J., Simon S. B., Simionovici A., See T. H., Robert F., Rietmeijer F. J. M., Rao W., Perronnet M. C., Papanastassiou D. A., Okudaira K., Ohsumi K., Ohnishi I., Nakamura-Messenger K., Nakamura T., Mostefaoui S., Mikouch T., Meibom A., Matrajt G., Marcus M. A., Leroux H., Lemelle L., Le L., Lanzirotti A., Langenhorst F., Krot A. N., Keller L. P., Kearsley A. T., Joswiak D., Jacob D., Ishii H., Harvey R., Hagiya K., Grossman L., Grossman J. N., Graham G. A., Gounelle M., Gillet P., Genge M. J., Flynn G., Ferroir T., Fallon S., Ebel D. S., Dai Z. R., Cordier P., Clark B., Chi M., Butterworth A. L., Brownlee D. E., Bridges J. C., Brennan S., Brearley A., Bradley J. P., Bleuet P., Bland P. A., and Bastien R. 2006. Mineralogy and petrology of comet 81P/Wild 2 nucleus samples. *Science* 314:1735–1739.
- Zolensky M., Nakamura-Messenger K., Rietmeijer F., Leroux H., Mikouchi T., Ohsumi K., Simon S., Grossman L., Stephan T., Weisberg M., Velbel M., Zega T., Stroud R., Tomeoka K., Ohnishi I., Tomioka N., Nakamura T., Matrajt G., Joswiak D., Brownlee D., Langenhorst F., Krot A., Kearsley A., Ishii H., Graham G., Dai Z. R., Chi M., Bradley J., Hagiya K., Gounelle M., and Bridges J. 2008. Comparing Wild 2 particles to chondrites and IDPs. *Meteoritics & Planetary Science* 43:261–272.
-